COMMUNICATION

An Ambient Pressure, Direct Hydrogenation of Ketones

Long Zhang, Zhiyao Lu, Andrew R. Rander, and Travis J. Williams*

Received 00th January 20xx,
Accepted 00th January 20xx

DOI: 10.1039/x0xx00000x

We report two bifunctional (pyridyl)carbene-iridium(I) complexes that catalyze ketone and aldehyde hydrogenation at ambient pressure. Aryl, heteroaryl, and alkyl groups are demonstrated, and mechanistic studies reveal an unusual polarization effect in which the rate is dependant of proton, rather than hydride, transfer. This method introduces a convenient, waste-free alternative to traditional borohydride and aluminum hydride reagents.

Direct hydrogenation of carbonyl groups is a 100% atom efficient, environmentally benign synthetic process. While hydride reagents like $LiAlH_4$ and $NaBH_4$ are effective and expedient for this transformation, these are accompanied by the cost and separation issues that accompany a stoichiometric portion of any metallic reagent, which makes direct hydrogenation an important option at scale.[1] Since Noyori's milestone discovery of asymmetric ketoester direct hydrogenation,[2] many well-defined molecular catalysts for hydrogenation, transfer hydrogenation, and dehydrogenation of C=O systems have emerged,[3] yet most rely on hydrogen gas pressure or a hydrogen donor/acceptor to obtain useful rates.[4] Frustrated Lewis-pair species have also been demonstrated,[5] although also rely on elevated gas pressure.[6] Such requirements for pressurization limit the utility of these methods and make them inconvenient for users without pressurization tools. Base metals (Fe, Co, Ni, and Cu) are emerging in this space;[7] in fact, the Hanson PNP–Co complexes catalyze ambient pressure hydrogenation of some ketones in THF at 60 °C,[7b] but room remains to introduce high reactivity, highly functional group tolerant catalysts for ambient pressure carbonyl hydrogenation. Thus, we report here a catalytic hydrogenation system that affects carbonyl hydrogenation with ambient hydrogen pressure at up to quantitative yield on a diverse set of ketones and aldehydes.

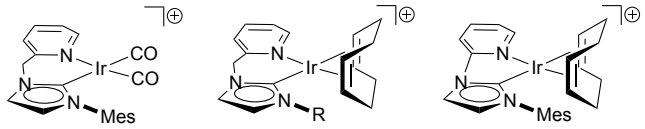

1 **2** R = Me **3** R = Mes **4**

Chart 1 Four iridium-based catalyst precursors. Anion = TfO^-.

We previously reported complexes **1**-**3** as pre-catalysis for glycerol dehydrogenation.[8] Therein we found that backbone deprotonation of **2** with concurrent pyridine dearomatization plays a mechanistic role in cleaving glycerol's O—H bond, apparently through a metal-ligand cooperative step. We further found that electron withdrawing CO ligands slowed dehydrogenation by comparing rates of reactions of **1** and **3**. We propose that the opposite should be true in the reductive direction, and that the apparent bifunctional nature of the backbone of **1**-**3** could facilitate H_2 cleavage as highlighted in Scheme 1.[3d]

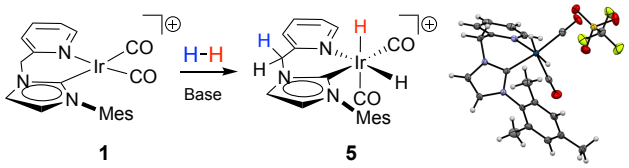

1 **5**

Scheme 1 Hydrogen molecule cleavage and dihydride iridium formation, ORTEP diagram of **5** (CCDC 2142636) with 50% ellipsoids.

When we treated precursor **1** with KO^tBu and one bar H_2 in a J. Young tube at room temperature, we found that it rapidly split hydrogen and formed iridium dihydride complex **5** (Scheme 1).[9] The same reaction is unsuccessful with iridium complex **4** that lacks a pyridyl methylene arm, which is consistent with our view that the backbone CH group is important to hydrogen cleavage.

Whereas complexes **1-3** cleave H_2 at ambient temperature and pressure as shown in Scheme 1, we screened them for

Donald P. and Katherine B. Loker Hydrocarbon Institute, Department of Chemistry, and Wrigley Institute for Environmental Studies, University of Southern California, Los Angeles, California 90089-1661, United States.
Email: travisw@usc.edu,

† Footnotes relating to the title and/or authors should appear here.

Electronic Supplementary Information (ESI) available: Synthesis and characterizations of all new compounds, kinetics studies, calculations, CIF data for **5**. CCDC 1438247 (**2**), 1438246 (**3**), 2142636 (**5**), and 2258133 (**6**) contain supplementary crystallographic data for the corresponding compounds. See DOI: 10.1039/x0xx00000x

ambient pressure acetophenone hydrogenation. Complex **1** has the highest reactivity among the three (Table S1). By contrast, complex **4** has no reactivity in acetone hydrogenation, again consistent with a role for the backbone CH group. Further consistent, none of these four iridium complexes has reactivity for acetone hydrogenation if base is removed from this reaction, although the role of the base could be to deprotonate a coordinated H_2 ligand. We therefore expect that ligand deprotonation and dearomatization play a role in hydrogen splitting and catalyst precursor activation for these precursors.

Condition optimization for the hydrogenation of acetophenone with **1** are outlined in Table S1. Various bases were tested for the hydrogenation of acetophenone, using 3 mol % **1**, 10 mol % base and 1 atm hydrogen pressure at 40 ° C. This taught us that effective bases have a pKa above ca. 16, which is appropriate for ligand backbone deprotonation: KO^{t}Bu, KH, and NaOEt afforded productive reaction where KOH and K_2CO_3 did not. We next turned to solvent and temperature. Increasing the temperature provided a modest increase in the reaction yield, but the yield at 120 ° C is lower than that at 100 ° C, thus leaving toluene as a suitable solvent for this reaction system. Gratifyingly, the system operates efficiently down to ambient pressure.

With optimized reaction conditions, we screened a series of ketones and aldehydes to understand the rection's scope. Studying a series of differentially *para*-substituted acetophenones (Table 1, entries 1-7) enabled calculation of a *negative* (nucleophilic substrate) Hammett reaction parameter of ρ = -0.93 (see Supporting Information). This negative ρ value is atypical for reduction, which should normally involve an electrophilic accepter receiving a nucleophilic hydride in a kinetically-relevant step: for example, the ρ value for $NaBH_4$ reduction of this reaction is +3.06,[10] and $LiAlH_4$ reduction of benzophenones +1.95.[11] Catalytic ketone hydrogenation with the Shvo system has ρ = +1.77, +0.91 under two conditions studied.[12,13] These undergo a concerted, outer-sphere hydrogen transfer mechanism. The ρ for Noyori type catalyst [$RuCl_2$(diphosphine)(1,2-diamine)] is ρ = +1.03.[14] Lewis acid-catalyzed acetophenone hydrogenation also has a positive ρ > 1.[15]

The negative ρ value in our system is consistent with kinetic relevance of a proton transfer step, rather than a hydride transfer as in the above cases. Its magnitude, ρ < -0.5, is consistent with the involvement of an anionic phenonone-containing fragment in or before our rate-limiting step.[16] Such a species could be a metal alkoxide,[17] which is protonated in a slow step (vide infra).

Continuing our study of substrate scope (Table 1), we examined ketones with increased steric demand. These are well tolerated (entries 8—9). Particularly, benzophenone was reduced at the larger 500 mg scale (entry 9b) to show that scaling the biphasic reaction does not significantly retard the yield. Furthermore, we tested the hydrogenation of benzophenone using conditions that did not involve our glove box, which we use for convenience in other cases. In entry 9c, all reagents were weighed out on the benchtop, and then the Schlenk flask was purged with H_2. This result shows that the

Table 1 Substrate scope.

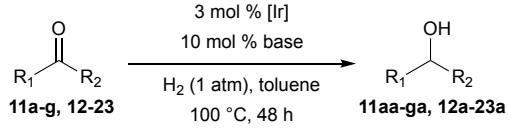

11a-g, 12-23 → **11aa-ga, 12a-23a**

Entry	Substrates	Products	[Ir]	Yield (%)[a]
1	R = H **11a**	R = H **11aa**	**1**	68
			6	>95
2	R = NMe_2 **11b**	R = NMe_2 **11ba**	**1**	>95
			6	>95
3	R = OMe **11c**	R = OCH_3 **11ca**	**1**	83
4	R = OH **11d**	R = OH **11da**	**1**	>95
5	R = Br **11e**	R = Br **11ea**	**1**	40
			6	81
6	R = Cl **11f**	R = Cl **11fa**	**1**	42
			6	83
7	R = NO_2 **11g**	R = NO_2 **11ga**	**1**	9[b]
8	**12**	**12a**	**1**	77
9	**13**	**13a**	**1**	85 77[c] 84[d]
10	**14**	**14a**	**1**	48
			6	88
11	**15**	**15a**	**1**	64
			6	89
12	**16**	**16a**	**1**	33
			6	72
13	**17**	**17a**	**1**	21
14	**18**	**18a**	**1**	73[b]

Entry	Substrates	Products	[Ir]	Yield (%)[a]
15	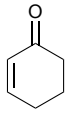 **19**	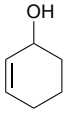 **19a**	**1**	32[b]
16	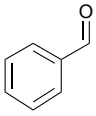 **20**	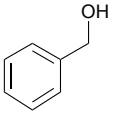 **20a**	**1**	>95
17	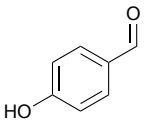 **21**	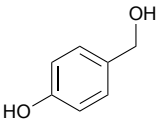 **21a**	**1**	>95
18	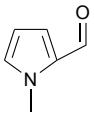 **22**	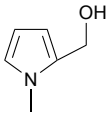 **22a**	**1** **6**	43[b] 85[b]
19	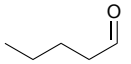 **23**	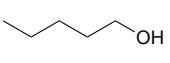 **23a**	**1** **6**	52[b] 80

[a]Isolated yield, 100 mg substrate scale. [b]NMR yield. [c]500 mg scale. [d]Reagents weighed out in air.

glove box is not necessary for this system, thus making it practically accessible to organic practitioners. Diphenylcyclopropenone was reduced chemoselectively at the C=O bond, with no evidence of C=C reduction (entry 10). Heteroaryl-substituted ketones and aldehydes were also hydrogenated (entries 11, 18). For aliphatic ketones such as 5-nonanone and 2,2,4,4-tetramethyl-3-pentanone, lower activity was observed (entries 12, 13).

To gain insight into the chemoselectivity of reactions of catalyst **1**, a competition experiment was performed in which a 1:1 mixture of styrene and benzaldehyde was hydrogenated using **1**. Benzaldehyde was hydrogenated more rapidly, with complete conversion of benzaldehyde and only 8% conversion of styrene observed over 48 hours. We can exploit this in the chemoselective reduction of enones (entries 14, 15), although cyclohexenone and cyclohexanone have low reactivity with this system. While highly chemoselective, entry 15 highlights a weakness of the method, which is that cyclohexanone and cyclopentanone substrates are low-yielding in our hands.

We also explored the activity of the complex **1** towards a collection of aldehydes. Benzaldehyde and 4-hydroxybenzaldehyde were reduced (entries 16, 17). Complex **1** has lower activity for heterocyclic aldehydes, possibly due to coordination of the heterocycle to the iridium center competing with H_2. While **1** operates efficiently with many substrates, we sought a faster and more efficient catalyst to address cases that are not well-served by **1**. Suspecting that carbonylation in **1** reduces the basicity of the intermediate that must receive a proton in the slow step, we designed and synthesized chloride-substituted pre-catalyst (CN)IrCl(CO), **6**. Single crystals of **6** were prepared from slow liquid diffusion of dichloromethane and diethyl ether to enable determination of its molecular structure (Scheme 2). Unlike Nozaki's pincer iridium system [κ^3-[2,6-(^{i}Pr$_2$PCH$_2$)$_2$(C$_6$H$_3$N)]IrH$_3$], which takes 20 hours to form its active iridium trihydride complex,[18] precursor **6** immediately transforms to trihydride **7** at ambient temperature and pressure (see Supporting Information). While it is somewhat less shelf-stable than **1**, we find that complex **6** enables more rapid reactions than **1**. Table 1 shows compared yields of hydrogenations with catalysts **1** and **6** in which the more rapid reactivity of **6** enables significantly superior performance.

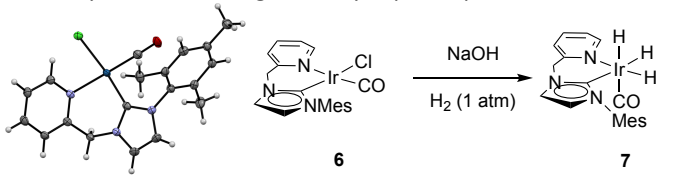

6 **7**

Scheme 2 Catalyst precursor **6** and iridium trihydride **7**.[18] ORTEP diagram of **6** (CCDC 2258133) with 50% ellipsoids.

A series of experiments were conducted to establish the reaction mechanism. We have measured the kinetic order of reaction for ketone, base, and catalyst and each is first order. We performed a kinetic isotope effect study by parallel reactions with complex **1** and benzophenone to investigate whether the H_2 coordinating step is rate-limiting. The observed KIE value of 1.06(11) is inconsistent with a kinetically relevant step involving H_2 metal complex coordination and cleavage; these typically have KIE > 2.[19] Further, hydrogen pressure does not effect this reaction rate. An Eyring plot, constructed using acetone as the substrate over a temperature range of 60-90 °C results in $\Delta S^{\ddagger}$ = -42.7(25) cal mol^{-1} K^{-1} and $\Delta H^{\ddagger}$ = 9.5(7) kcal mol^{-1} (see Supporting Information). This indicates a very low enthalpic (bond cleavage) component, but a significant entropic cost, in or before the rate-limiting transition state. We see this body of data as consistent with a reversible H_2 activation and a fast, facile hydride transfer early in the mechanism, both preceding a slow proton transfer to alkoxide or alcohol dissociation step. While the strong $\Delta S^{\ddagger}$ fits with rate-limiting gas activation, kinetic independence of [H_2] leads us to explain this as an intramolecular proton shutte. Thus, the ratio of reaction rates with and without added alcohol, $k_{iPrOH}/k_{no\ iPrOH}$ = 1.625, illustrates that added isopropanol accelerates the reaction overall, which is consistent with a role of for the alcohol as a proton shuttle in a rate-limiting proton transfer. In our previous work, we calculated the energetic advantage of such a proton shuttle in ketone hydrogenation by an analogous bifunctional iridium complex.[20]

We advance the mechanistic hypothesis shown in Scheme 3. We propose that species **5** transfers a hydride to substrate in a kinetically invisible step to form proposed intermediate **8**. Then, a kinetically relevant proton transfer from the catalyst's methylene arm to the alkoxide occurs. We suspect that an equivalent of alcohol or the protonated conjugate acid of the base is involved in this step as a proton shuttle, sketched as **9**. A neutral alcohol is then formed and released. We propose that the slow step is in this proton transfer/ alcohol dissociation sequence. Next, we believe that H_2 coordinates to the

dearomatized iridium species to form a structure like **10**. A proton can then be transferred from H_2 to the ligand backbone to regenerate the aromatized iridium-dihydride **5** in a reaction analogous to the one we observe stoichiometrically in scheme 1. Again, a proton shuttle would be logical.

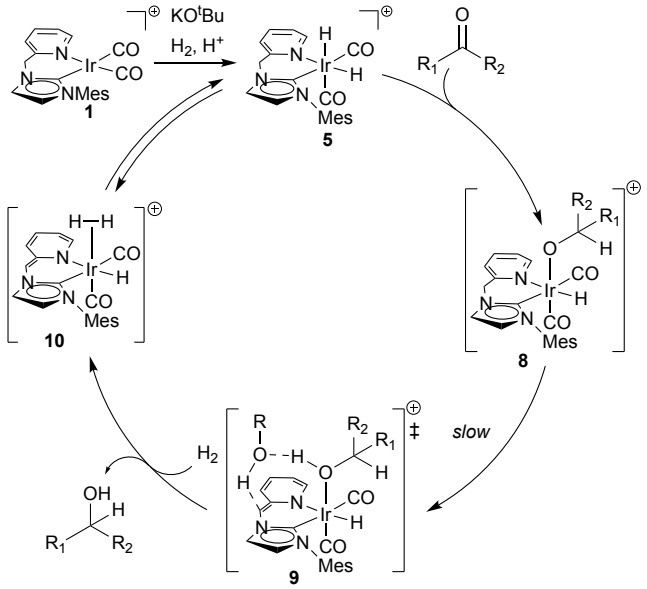

Scheme 3 Proposed mechanism of catalysis.

In conclusion, we have developed efficient iridium catalysts **1** and **6** for the hydrogenation of ketones and aldehydes at ambient pressure. Importantly, finding a kinetic scheme in which H_2 is zero order enables facile ambient pressure reactions, which avoid the use of expensive autoclave reactors that are not readily available in every lab. Further, reactions can be accomplished using traditional Schlenk techniques without need for a glove box or freeze-pump-thaw conditions. These attributes improve the safety and operational convenience of the reaction. Complex, **6**, which differs from **1** by substitution of a CO for a chloride, has higher catalytic hydrogenation reactivity, affording useful results for some systems that are not easily reduced with **1**. We envision these catalysts as useful tools both for organic synthesis at scale, where the by-product of $NaBH_4$ or $LiAlH_4$ reduction creates operational costs and challenges, or small-scale practitioners needing to eliminate by-product separation, as in radiopharmaceutical synthesis.

Conflict of interest

TJW and ZL are co-founders of a company, Catapower Inc, which sells complexes **1**-**3**.

Acknowledgements

This work was supported by the National Science Foundation, CHE-1856395. We thank the NSF (CHE-2018740, DBI-0821671, CHE-0840366), the NIH (S10 RR25432), and USC Research and Innovation Instrumentation Awards for analytical tools.

References

1 H. -U. Blaser, C. Malan, B. Pugin, F. Spindler, H. Steiner and M. Studer, *Advanced Synthesis & Catalysis*, 2003, **345**, 103–151.
2 R. Noyori and T. Ohkuma, *Angew. Chem. Int. Ed.*, 2001, **40**, 40–73.
3 For selected reviews: (a) S. E. Clapham, A. Hadzovic and R. H. Morris, *Coord. Chem. Rev.*, 2004, **248**, 2201–2237; (b) G. E. Dobereiner and R. H. Crabtree, *Chem. Rev.*, 2010, **110**, 681–703; (c) B. L. Conley, M. K. Pennington-Boggio, E. Boz and T. J. Williams, *Chem. Rev.*, 2010, **110**, 2294–2312; (d) C. Gunanathan and D. Milstein, *Accounts Chem. Res.*, 2011, **44**, 588–602; (e) P. A. Dub and J. C. Gordon*, ACS Catal.*, 2017, **7**, 6635–6655; (f) J. Wen, F. Wang and X. Zhang, *Chem. Soc. Rev.*, 2021, **50**, 3211–3237; (g) Cherepakhin, V., Williams, T. J. *Synthesis*, 2021, **53**, 1023-1034.
4 (a) C. A. Sandoval, T. Ohkuma, K. Muñiz and R. Noyori, *J. Am. Chem. Soc.*, 2003, **125**, 13490–13503; (b) C. P. Casey and H. Guan, *J. Am. Chem. Soc.*, 2007, **129**, 5816–5817; (c) R. Langer, G. Leitus, Y. Ben-David and D. Milstein, *Angew. Chem. Int. Ed.*, 2011, **50**, 2120–2124; (d) G. Zhang, B. L. Scott and S. K. Hanson, *Angew. Chem.*, 2012, **124**, 12268–12272; (e) P. O. Lagaditis, P. E. Sues, J. F. Sonnenberg, K. Wan, A. J. Lough and R. H. Morris, *J. Am. Chem. Soc.*, 2014, **136**, 1367–1380; (f) B. Butschke, M. Feller, Y. Diskin-Posner and D. Milstein, *Catal. Sci. Tech.*, 2016, **6**, 4428–4437.
5 D. J. Scott, M. J. Fuchter and A. E. Ashley, *Chem. Soc. Rev.*, 2017, **46**, 5689–5700.
6 S. Wei and H. Du, *J. Am. Chem. Soc.* 2014, **136**, 12261–12264.
7 (a) S. S. Christine, F. Freutel, A. J. Lough and R. H. Morris, *Angew. Chem. Int. Ed.*, 2008, **47**, 940–943.; (b) G. Zhang, B. L. Scott and S. K. Hanson, *Angew. Chem. Int. Ed.*, 2012, **51**, 12102–12106; (c) Y. Hamada, Y. Koseki, T. Fujii, T. Maeda, T. Hibino and K. Makino, *Chem. Commun.*, 2008, **46**, 6206–6208; (d) S. W. Krabbe, M. A. Hatcher, R. K. Bowman, M. B. Mitchell, M. S. McClure and J. S. Johnson, *Org. Lett.*, 2013, **15**, 4560–4563.
8 Z. Lu, I. Demianets, R. Hamze, N. J. Terrile, and T. J. Williams, *ACS Catal.*, 2016, **6**, 2014-2017.
9 V. K. Do, N. Alfonso Vargas, A. J. Chavez, L. Zhang, V. Cherepakhin, Z. Lu, R. P. Currier, P. A. Dub, J. C. Gordon and T. J. Williams, *Catal. Sci. Tech.*, 2022, **12**, 7182–7189.
10 K. Bowden and M. Hardy, *Tetrahedron*, 1966, **22**, 1169-1174.
11 K. E. Wiegers and S. G. Smith, *J. Am. Chem. Soc.*, 1977, **99**, 1480-1487.
12 C. P. Casey, N. A. Strotman, S. E. Beetner, J. B. Johnson, D. C. Priebe and I. A. Guzei, *Organometallics*, 2006, **25**, 1236-1244.
13 L. Koren-Selfridge, H. N. Londino, J. K. Vellucci, B. J. Simmons, C. P. Casey and T. B. Clark, *Organometallics*, 2009, **28**, 2085-2090.
14 C. A. Sandoval, Q. Shi, S. Liu and R. Noyori, *Chem. Asian J.*, 2009, **4**, 1221-1224.
15 D. J. Parks and W. E. Piers, *J. Am. Chem. Soc.*, 1996, **118**, 9440-9441.
16 R. Stewart and K. Yates, *J. Am. Chem. Soc.*, 1958, **80**, 6355-6359.
17 J. Xu, T. Wei, and Q. Zhang, *J. Org. Chem.*, 2004, **69**, 6860-6866.
18 R. Tanaka, M. Yamashita and K. Nozaki, *J. Am. Chem. Soc.*, 2009, **131**, 14168–14169.
19 C. R. Landis and T. W. Brauch, *Inorg. Chim. Acta*, 1998, **270**, 285–297.
20 I. Demianets, V. Cherepakhin, A. Maertens, P. J. Lauridsen, S. Mallikarjun Sharada and T. J. Williams, *Polyhedron*, 2020, **182**, 114508.

Supporting Information

An Ambient Pressure, Direct Hydrogenation of Ketones

Long Zhang, Zhiyao Lu, Andrew R. Rander, Travis J. Williams*

Donald P. and Katherine B. Loker Hydrocarbon Institute and Department of Chemistry, University of Southern California, Los Angeles, California 90089-1661, United States

*travisw@usc.edu

Table of Contents

I. General Procedures

All air and water sensitive procedures were carried out either in a Vacuum Atmosphere glove box under nitrogen (2-10 ppm O_2 for all manipulations) or using standard Schlenk techniques under nitrogen. Deuterated NMR solvents were purchased from Cambridge Isotopes Laboratories. Unless otherwise stated, all reagents were purchased from major commercial suppliers (Sigma-Aldrich, Merck, Fluorochem, Apollo Scientific, Fischer Scientific, Tokyo Chemical Industry, Acros Organics) and used without further purification. Dichloromethane, acetonitrile and hexanes are purchased from VWR and dried in a J. C. Meyer solvent purification system with alumina/copper(II) oxide columns; toluene was dried using sodium benzophenone ketyl; dichloromethane was dried by vacuum transfer from a calcium hydride suspension; chloro(1,5-cyclooctadiene)iridium(I) dimer (Strem), sodium trifluoromethanesulfonate (Sigma-Aldrich), potassium tert-butoxide (Sigma-Aldrich) were purged with nitrogen and stored under nitrogen atmosphere; pyridine-imidazolium ligands and corresponding silver carbenes were synthesized using a literature procedure.[1] CO was supplied by Airgas through USC Mailing and Material Management.

NMR spectra were recorded on a Varian Mercury 400, Varian VNMRS 500, or VNMRS 600, spectrometers processed using MestReNova. All chemical shifts are reported in units of ppm and referenced to the residual ^{1}H or ^{13}C solvent peak and line-listed according to (s) singlet, (bs) broad singlet, (d) doublet, (t) triplet, (dd) double doublet, etc. ^{13}C spectra are delimited by carbon peaks, not carbon count. ^{19}F chemical shifts are referenced to a trichlorofluoromethane external (coaxial insert tube) standard (0 ppm). Air-sensitive NMR spectra were taken in 8" J-Young tubes (Wilmad or Norell) with Teflon valve plugs. Data were collected and graphed was plotted with Microsoft Excel.

Hydrogenation Procedures

The iridium catalysts for carbonyl groups hydrogenation are stored in a glovebox for long term purpose. In a typical reaction, iridium catalyst, base (i.e. KOtBu) and solid substrates are weighed inside the glovebox, added to a Schlenk flask equipped with a magnetic stir bar. (Figure S1) Liquid substrates and toluene are measured and added to the same flask with a disposable plastic syringe. An oil bath is used for reactions at 100 °C. Bath temperature is monitor using an alcohol thermometer. Normally < ±2.5 °C temperature fluctuation is observed for oil baths.

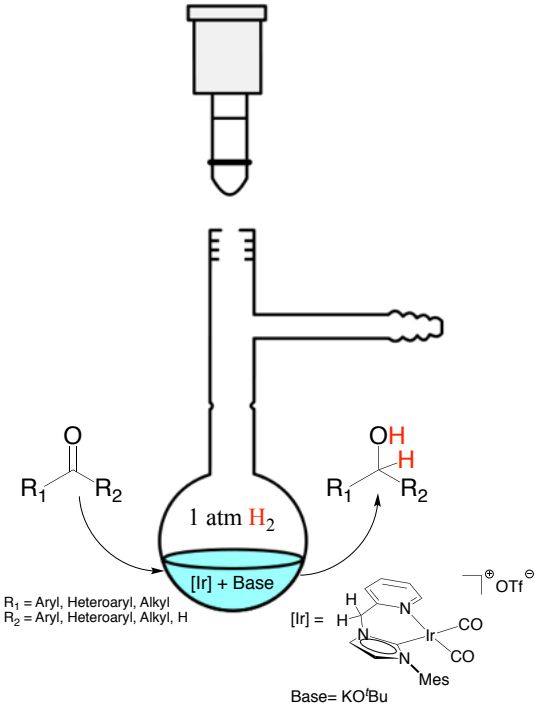

Figure S1. Apparatus set up for hydrogenation reactions.

II. Controlled experiments for the hydrogenation of acetophenone

Different conditions were tried to optimize the hydrogenation of acetophenone. Complex **1**—**4** has been screened for catalytic hydrogenation under ambient pressure. In a typical reaction, the solvent of the resulting solution was removed in vacuum and 5 mL saturated NaCl solution was added into the residue. The resulting mixture was extracted with DCM (3 times, 15 mL) and concentrated under reduced pressure. The residue was dissolved in deuterated chloroform and analyzed by NMR. The NMR yields were obtained by quantitative ^{1}H NMR analysis using mesitylene as the internal standard.

Table S1. Optimization of the hydrogenation of acetophenone.

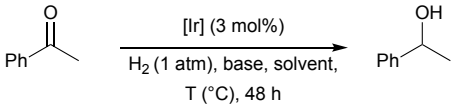

Entry	[Ir]	base	solvent	T (°C)	NMR yield (%)
1	**1**	KO^{t}Bu	toluene	40	40
2	**2**	KO^{t}Bu	toluene	40	<5
3	**3**	KO^{t}Bu	toluene	40	13
4	**4**	KO^{t}Bu	toluene	40	0
5	**1**	K_2CO_3	toluene	40	<5
6	**1**	NaOEt	toluene	40	37
7	**1**	KOH	toluene	40	8
8	**1**	KH	toluene	40	11
9	**1**	—	toluene	40	0
10	**1**	KO^{t}Bu	benzene	40	13
11	**1**	KO^{t}Bu	THF	40	<5
12	**1**	KO^{t}Bu	MeOH	40	5
13	**1**	KO^{t}Bu	toluene	60	46
14	**1**	KO^{t}Bu	toluene	80	78
15	**1**	KO^{t}Bu	toluene	100	88
16	**1**	KO^{t}Bu	toluene	120	61

III. Preparation of catalyst

Note: all the procedures for syntheses of iridium complexes are performed in the glovebox.

*Complex **4***

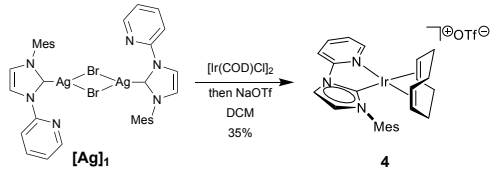

$[Ag]_1$ **4**

In the glovebox under nitrogen, in a 100 mL Schlenk flask wrapped in foil to avoid light, dibromo-di(3-mestiyl-1*H*-imidazol-2-ylidene)-disilver(I) (100 mg, 0.111 mmol)[2] was added in small portions to a stirring solution of chloro(1,5-cyclooctadiene)Iridium(I) dimer (74.6 mg, 0.222 mmol) in dry dichloromethane (20 mL). After 6 hours, sodium trifluoromethanesulfonate (38.2 mg, 0.222 mmol) was also added to the mixture. After stirring for 30 minutes, the solution was filtered through a dry pad of celite to remove the byproducts. The solvent was evaporated under reduced pressure to yield a red glassy solid. This red solid was dissolved in dry dichloromethane (10 mL), and dry hexanes (20 mL) was added to the solution to facilitate a precipitation. A red crystalline solid was acquired and dried under vacuum (54 mg, 35%). This sample was spectroscopically pure by ^{1}H NMR (Figure S2).

This synthetic step can be done without a glove box. Pyridine-imidazolium ligands were synthesized in a laboratory reflux apparatus out of the glove box. For $[Ag]_1$ synthesis in air, pyridine-imidazolium ligand (500 mg, 1.59 mmol), Ag_2O (221.5mg, 0.96 mmol, 0.6 eq) and dichloromethane (50 mL) were added in a 250 mL round bottom flask wrapped in foil. This flask was purged with N_2 and connected with a N_2 balloon. After stirring for 48 hours, the solution was filtered through a pad of celite to remove the unreacted Ag_2O and byproducts. Half of the solvent was evaporated under reduced pressure and then hexanes (50 mL) was dropped into this solution using a pressure-equalizing dropping funnel. The top of the dropping funnel is connected with a N_2 balloon. A grey crystalline solid was acquired and dried under vacuum (520 mg, 77.6%).

For complex **4** synthesis in air, in a 100 mL round bottom flask, chloro(1,5-cyclooctadiene)Iridium(I) dimer (100 mg, 0.3 mmol) was dissolved in dichloromethane (10 mL). Then, using a pressure-equalizing dropping funnel to drop a solution of $[Ag]_1$ (134 mg, 0.15 mmol) in dichloromethane (10 mL) into this stirring solution. The apparatus was equipped with an N_2 balloon. After 6 hours, sodium trifluoromethanesulfonate (51.2 mg, 0.3 mmol) was also added to the mixture. After stirring for another 30 minutes, the solution was filtered through a pad of celite to remove byproducts. Half of the solvent was evaporated under reduced pressure and then hexanes (25 mL) was dropped into this solution using a pressure-equalizing dropping funnel. The top of the dropping funnel is connected with a N_2 balloon. A red solid was acquired and dried under vacuum (68 mg, 33%).

^{1}H NMR (500 MHz, cdcl$_3$) δ 8.64 (t, *J* = 1.7 Hz, Im 1H), 8.59 (d, *J* = 8.4 Hz, py 1H), 8.33 (t, *J* = 7.9 Hz, py 1H), 8.04 (d, *J* = 5.7 Hz, py 1H), 7.54 – 7.48 (m, py 1H), 7.01 (s, mesityl-ar 2H), 6.86 (d, *J* = 2.1 Hz, Im 1H), 4.91 – 4.71 (m, COD sp^2 2H), 3.77 – 3.56 (m, COD sp^2 2H), 2.37 (s, mesityl-para-methyl 3H), 2.21 (d, *J* = 12.5 Hz, COD sp^3 4H), 2.13 – 2.11 (s, mesityl-ortho-methyl 6H) 2.01 – 1.83 (m, COD sp^3 4H).

^{13}C NMR (126 MHz, cdcl$_3$) δ 172.87 (carbene *C*), 154.55 (py), 147.49 (py), 144.99 (py), 141.00 (mesityl-ar), 134.37 (mesityl-ar), 133.64 (mesityl-ar), 130.01 (mesityl-ar), 125.81 (Im), 124.40 (py), 119.53 (Im), 114.33 (py), 86.42 (COD sp^2), 65.99 (COD sp^2), 33.80 (COD sp^3), 29.24 (COD sp^3), 21.41 (mesityl-*C*H$_3$), 17.74 (mesityl-*C*H$_3$), 14.27 (mesityl-*C*H$_3$).

IR (thin film/cm-1) ν 3533, 3109, 3052, 2914, 2831, 1734, 1591, 1570, 1470, 1435, 1394, 1263, 1223, 1150, 1030, 730, 700, 636.

MS (MALDI) calc'd for $[C_{25}H_{29}IrN_3]^+$ 563.7, found 563.2.

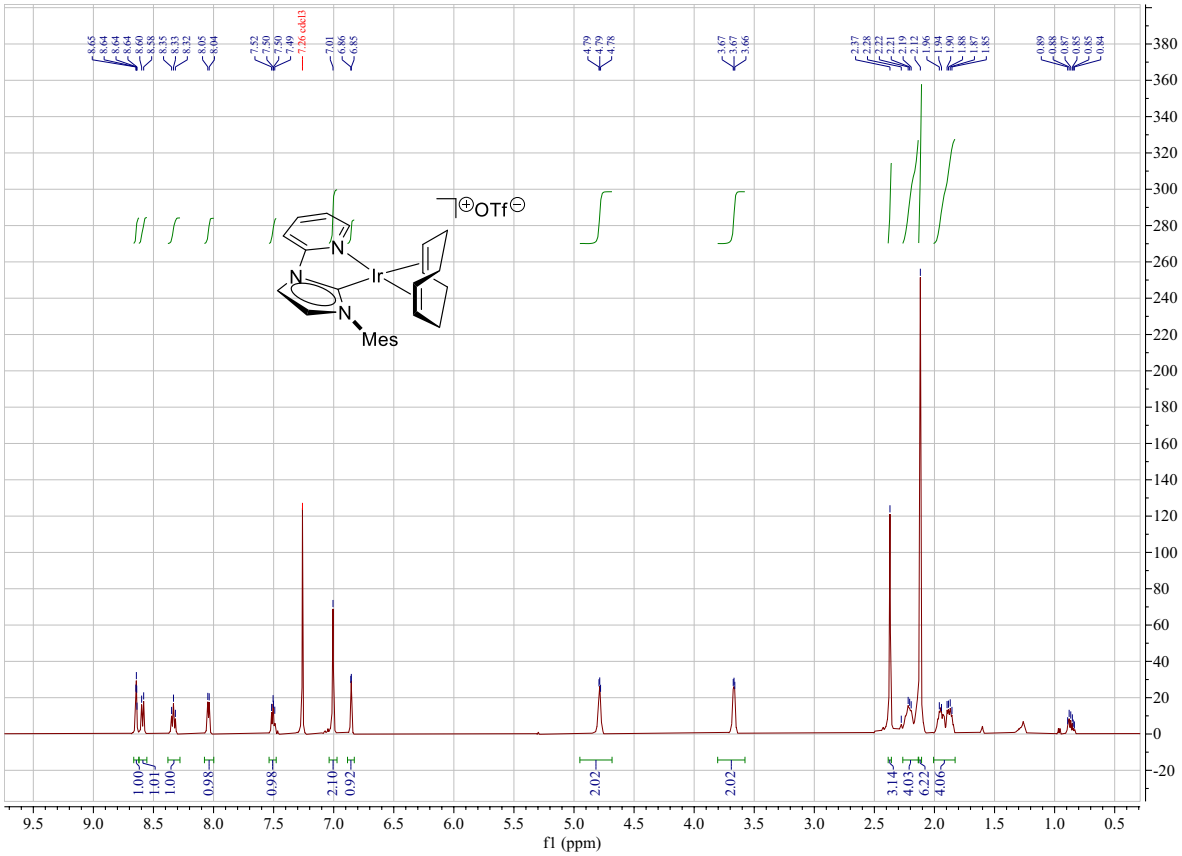

Figure S2. ^{1}H NMR spectrum of complex **4** at 25 °C in $CDCl_3$.

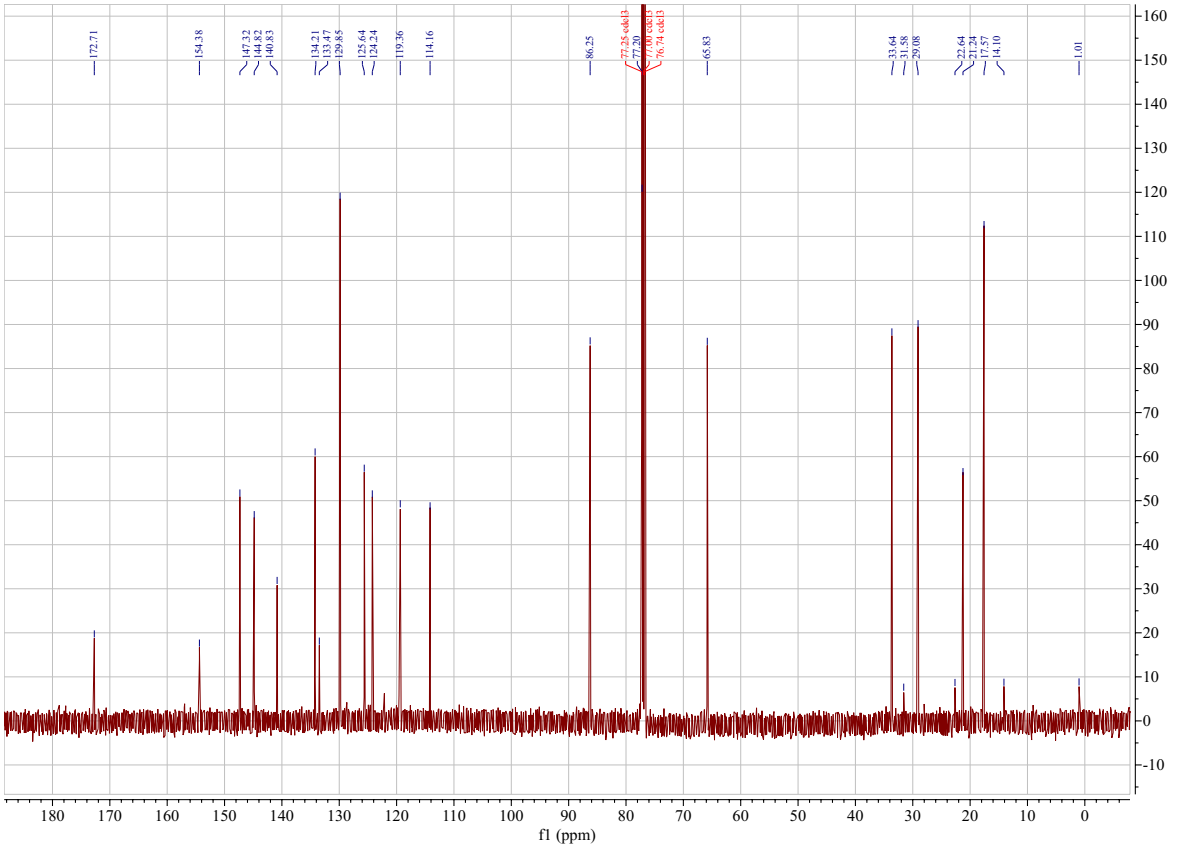

Figure S3. ^{13}C NMR spectrum of complex **4** at 25 °C in $CDCl_3$.

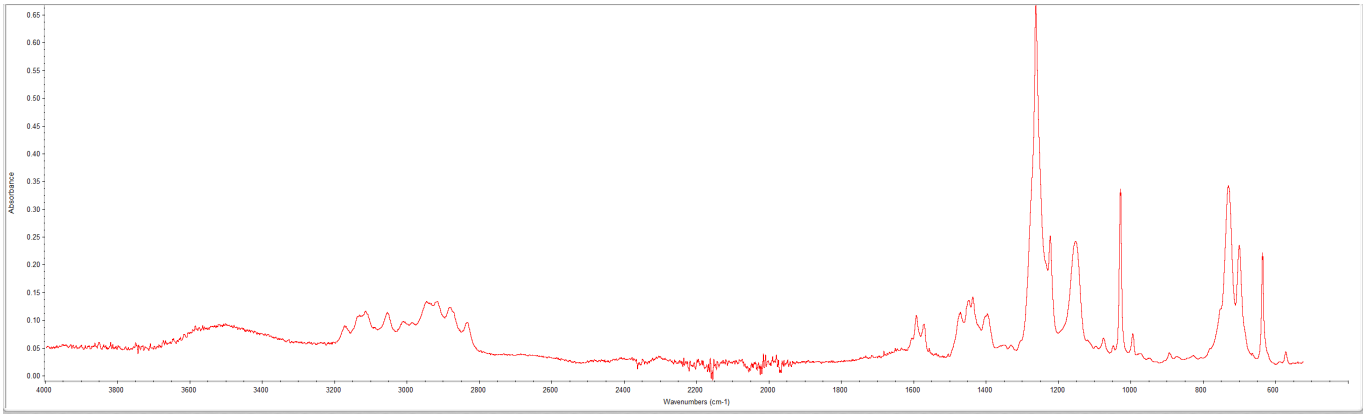

Figure S4. Infrared spectrum of complex **4**.

*Complex **6***

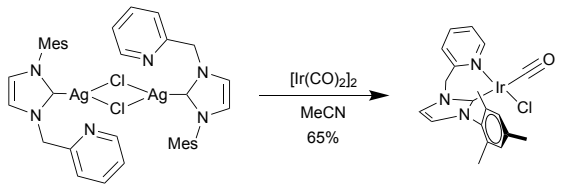

[Ag]$_2$ **6**

In the glovebox under nitrogen, in a 100 mL Schlenk flask, chloro(1,5-cyclooctadiene)iridium(I) dimer (100 mg, 0.15 mmol) was dissolved in dry acetonitrile (20 mL). The flask was purged with 1 atm CO gas. After 5 min, dichloro-di(1-(2,4,6-trimethylphenyl)-3-(2-picolyl)-imidazol-2-ylidene)-disilver(I)[2] ([Ag]$_2$, 125 mg, 0.15 mmol) was added in small portions to this stirring solution. After stirring for 1 hour, the solution was filtered through a tube of dry cotton, apparently to remove the silver chloride byproduct. The solvent was evaporated under reduced pressure to yield a yellow glassy solid. This yellow solid was dissolved in dry dichloromethane (10 mL), and dry hexanes (20 mL) was added to the solution to facilitate a precipitation. A yellow crystalline solid was acquired and dried under vacuum (104 mg, 65%). This sample was spectroscopically pure by ^{1}H NMR (Figure S6).

This synthetic step can be done without a glove box. [Ag]$_2$ can be synthesized out in air and the procedure is the same as the steps mentioned in preparation of complex **4**.

For complex **6** synthesis out in air, chloro(1,5-cyclooctadiene)iridium(I) dimer (100 mg, 0.15 mmol) was dissolved in acetonitrile (20 mL) in a 100 mL Schlenk flask. After 5 min, using a pressure-equalizing dropping funnel to drop a solution of [Ag]$_2$ (125 mg, 0.15 mmol) in acetonitrile (10 mL) into this stirring solution. After 1 hour, the solution was filtered through a pad of celite to remove byproducts. The solvent was evaporated under reduced pressure to yield a yellow glassy solid. This yellow solid was dissolved in dichloromethane (10 mL) and then hexanes (25 mL) was dropped into this solution using a pressure-equalizing dropping funnel. The top of the dropping funnel is connected with a N_2 balloon. A yellow solid was acquired and dried under vacuum (93 mg, 58%).

^{1}H NMR (500 MHz, cd_2cl_2) δ 9.31 (dd, *J* = 5.8, 1.7 Hz, py 1H), 7.97 (td, *J* = 7.7, 1.7 Hz, py 1H), 7.59 (d, *J* = 7.8 Hz, py 1H), 7.51 (dd, *J* = 7.5, 5.9 Hz, py 1H), 7.22 (d, *J* = 2.1 Hz, Im 1H), 7.03 (s, mesityl-ar 2H), 6.82 (d, *J* = 2.1 Hz, Im 1H), 5.38 – 5.36 (s, methylene 2H), 2.39 (s, mesityl-para-methyl 3H), 2.10 (s, mesityl-ortho-methyl 6H).

^{13}C NMR (126 MHz, cd_2cl_2) δ 176.02 (carbene *C*), 162.09 (CO), 154.13 (py), 153.58 (py), 139.81 (py), 139.60 (mesityl), 136.26 (py), 135.97 (mesityl), 129.32 (mesityl), 125.05 (py), 123.92 (mesityl), 121.31 (Im), 120.38 (Im), 55.42 (py-CH_2), 21.25 (mesityl-CH_3), 18.64 (mesityl-CH_3).

IR (thin film/cm-1) ν 3055, 2992, 2939, 2252 (CO), 1558, 1505, 1435, 1416, 1374, 1270, 1035, 917, 734, 702.

MS (MALDI) calc'd for $[C_{18}H_{19}IrN_3]^+$ 469.6, found 469.7.

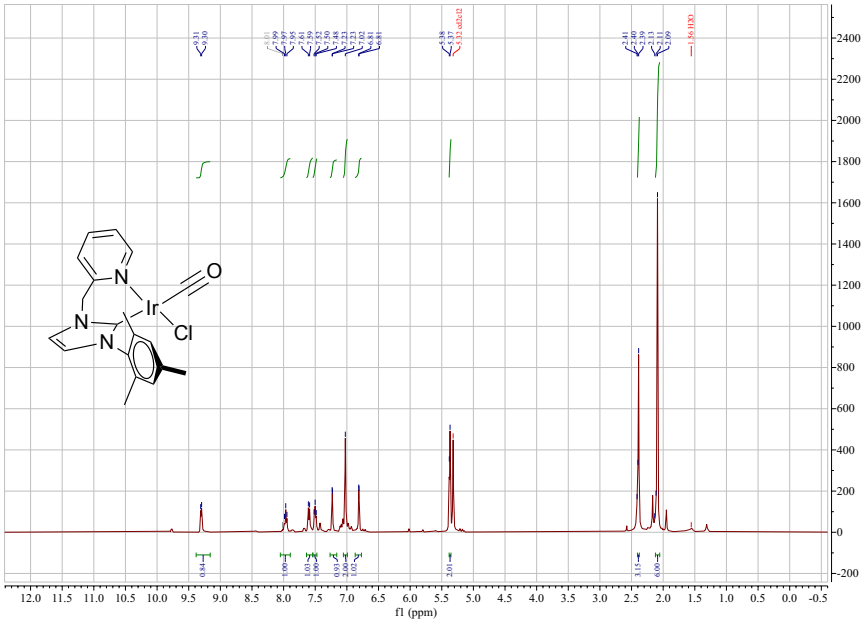

Figure S5. ^{1}H NMR spectrum at 25 °C in CD_2Cl_2.

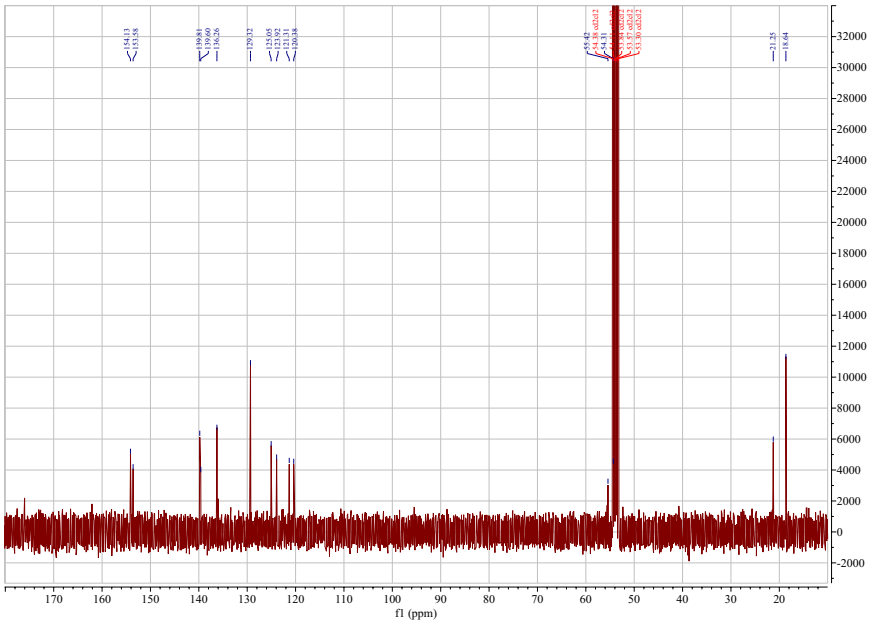

Figure S6. ^{13}C spectrum at 25 °C in CD_2Cl_2.

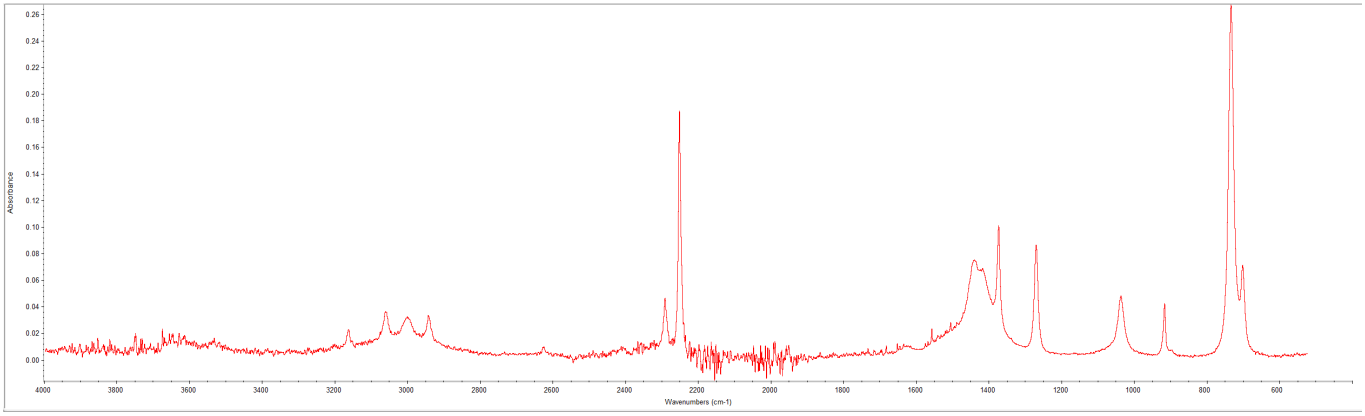

Figure S7. Infrared spectrum of complex **6**.

IV. NMR Spectra of products in Table 1

All compounds formed in Table 1 are known compounds, and most are commercially available.

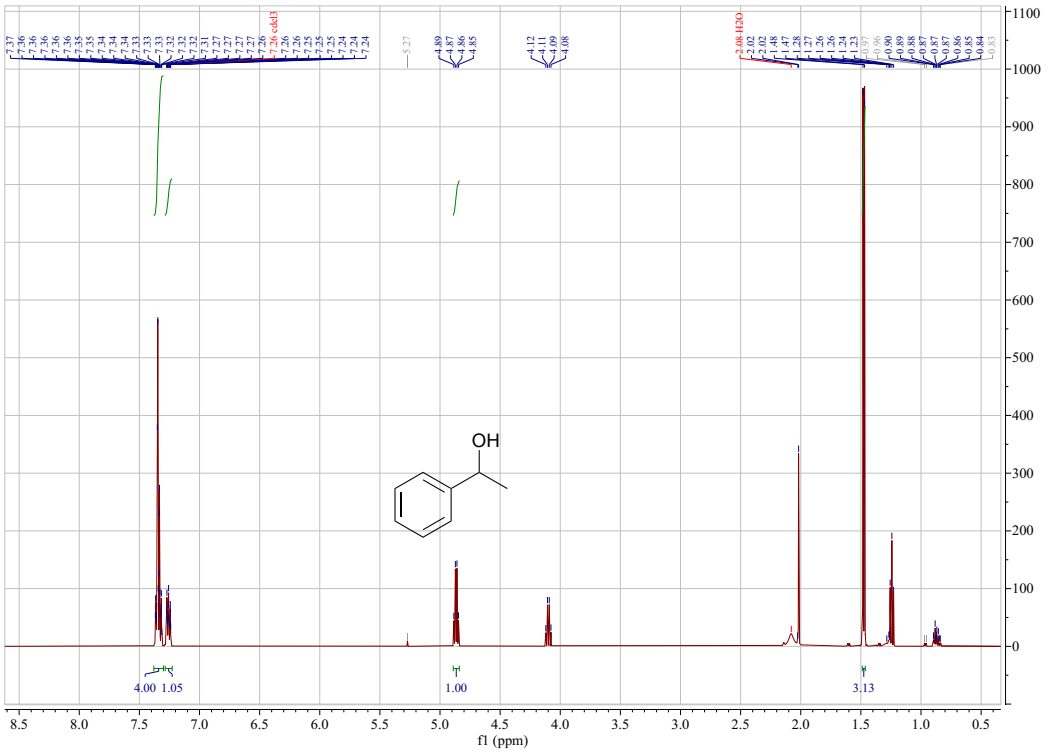

^{1}H NMR (500 MHz, cdcl$_3$) δ 7.38 – 7.30 (m, 4H), 7.28 – 7.24 (m, 1H), 4.87 (q, *J* = 6.5 Hz, 1H), 1.48 (d, *J* = 6.4 Hz, 3H).

Figure S8. ^{1}H NMR spectrum of Table 1 Entry 1 product **11aa** in $CDCl_3$. Data are consistent with a commercial compound.

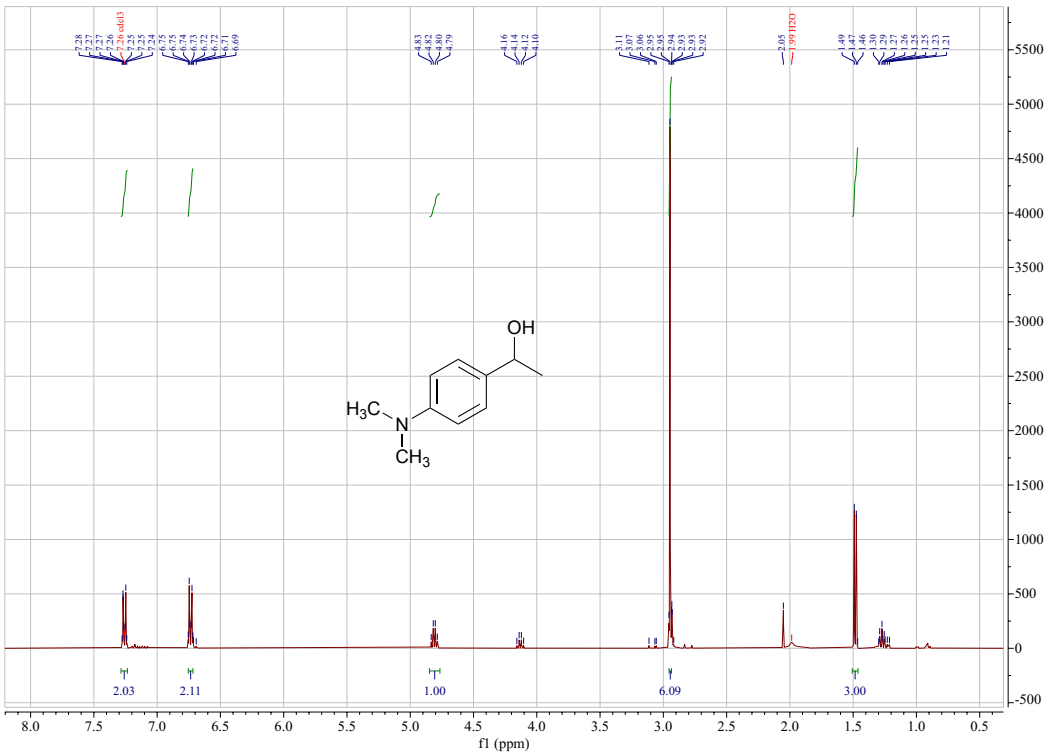

^{1}H NMR (400 MHz, cdcl$_3$) δ 7.30 – 7.25 (m, 2H), 6.78 – 6.73 (m, 2H), 4.82 (q, *J* = 6.4 Hz, 1H), 2.96 (s, 6H), 1.50 (d, *J* = 6.4 Hz, 3H).

Figure S9. ^{1}H NMR spectrum of Table 1 Entry 2 product **11ba** in $CDCl_3$. Data are consistent with a commercial compound.

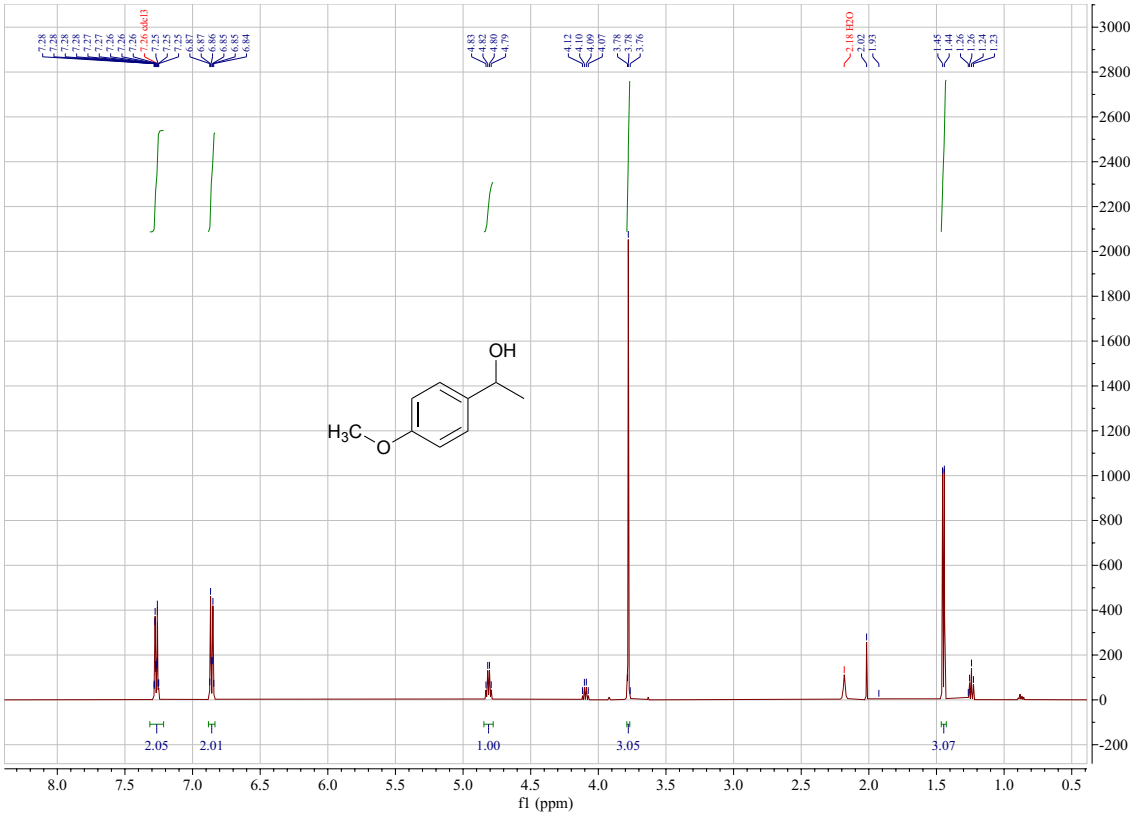

^{1}H NMR (500 MHz, cdcl$_3$) δ 7.29 – 7.24 (m, 2H), 6.88 – 6.83 (m, 2H), 4.81 (q, *J* = 6.4 Hz, 1H), 3.78 (s, 3H), 1.45 (d, *J* = 6.4 Hz, 3H).

Figure S10. ^{1}H NMR spectrum of Table 1 Entry 3 product **11ca** in $CDCl_3$. Data are consistent with a commercial compound.

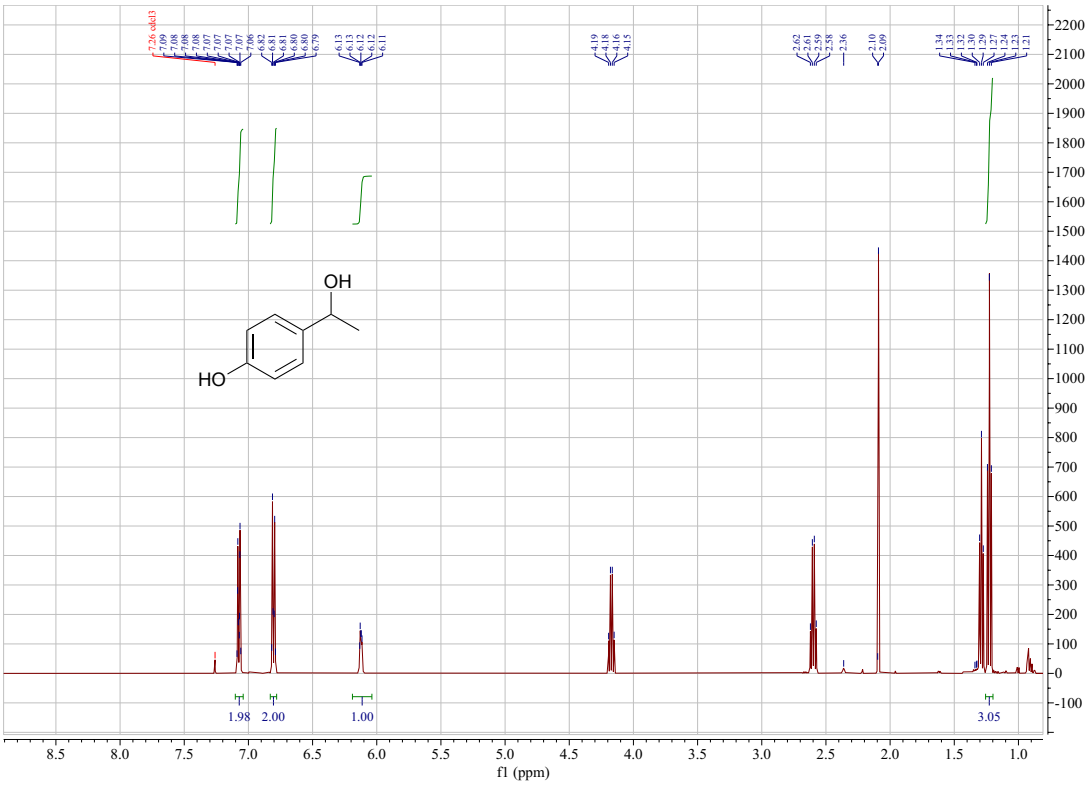

^{1}H NMR (500 MHz, cdcl$_3$) δ 7.10 – 7.04 (m, 2H), 6.84 – 6.78 (m, 2H), 6.15 – 6.09 (q, 1H), 1.23 (m, *J* = 7.6 Hz, 3H).

Figure S11. ^{1}H NMR spectrum of Table 1 Entry 4 product **11da** in $CDCl_3$. Data are consistent with a commercial compound.

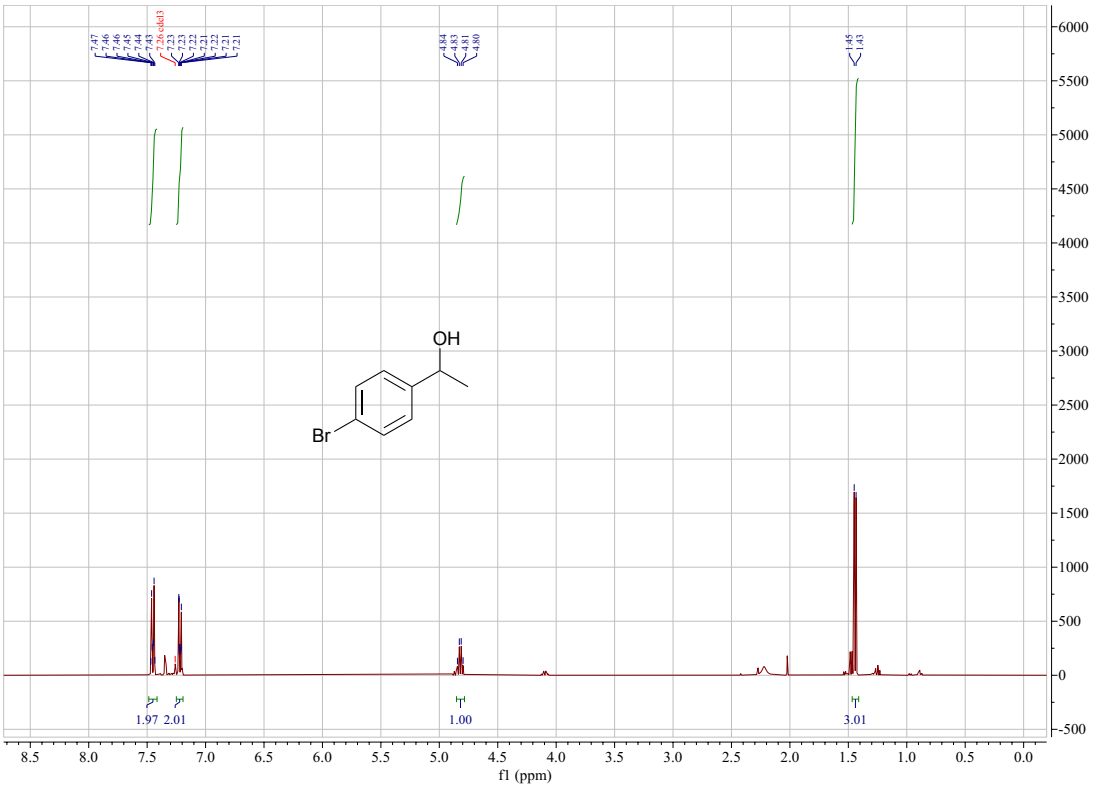

^{1}H NMR (400 MHz, cdcl$_3$) δ 7.53 – 7.46 (m, 2H), 7.28 – 7.22 (m, 2H), 4.86 (q, *J* = 6.5 Hz, 1H), 1.48 (d, *J* = 6.5 Hz, 3H).

Figure S12. ^{1}H NMR spectrum of Table 1 Entry 5 product **11ea** in $CDCl_3$. Data are consistent with a commercial compound.

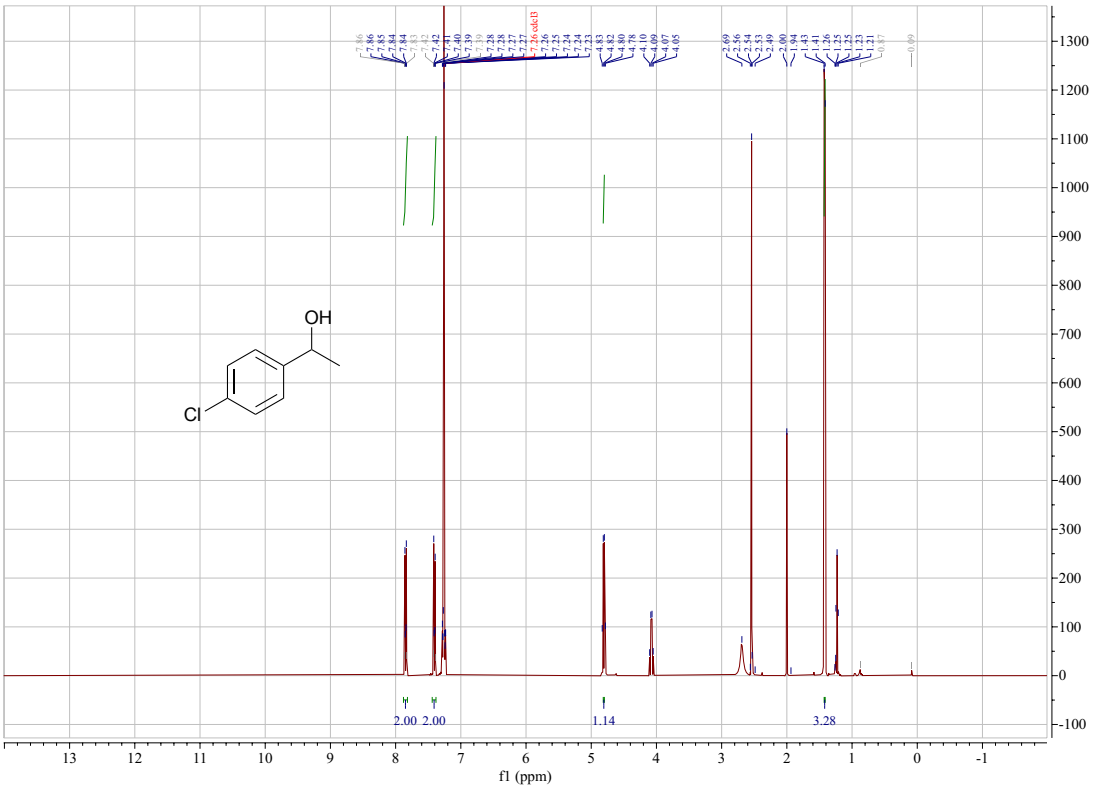

^{1}H NMR (400 MHz, cdcl$_3$) δ 7.83 – 7.86 (m, 2H), 7.39 – 7.42 (m, 2H), 4.82 (q, *J* = 6.4 Hz, 1H), 1.41 (d, *J* = 6.4 Hz, 3H).

Figure S13. ^{1}H NMR spectrum of Table 1 Entry 6 product **11fa** in $CDCl_3$. Data are consistent with a commercial compound.

Entry 7 product **11ga**:

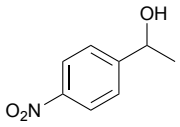

^{1}H NMR (600 MHz, cdcl$_3$) δ 8.17 – 8.13 (m, 2H), 7.55 – 7.50 (m, 2H), 5.01 (q, *J* = 6.5 Hz, 1H), 1.50 (d, *J* = 6.5 Hz, 3H).

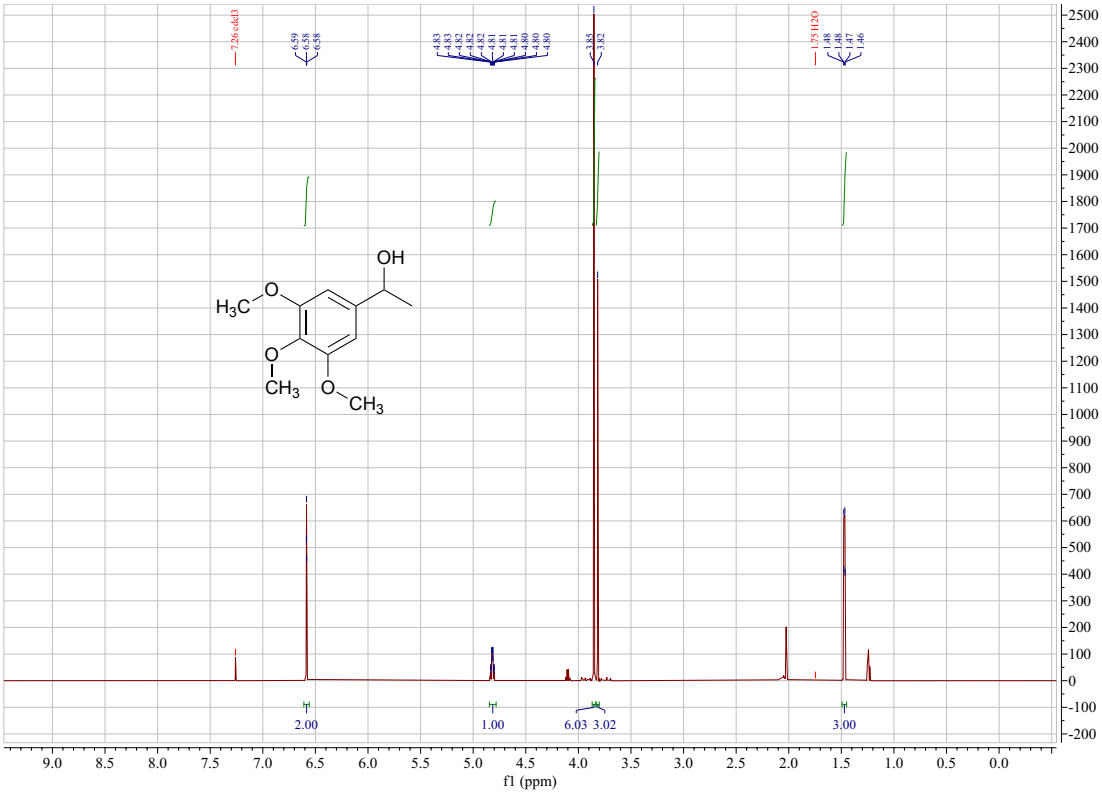

^{1}H NMR (600 MHz, cdcl$_3$) δ 6.58 (t, *J* = 0.7 Hz, 2H), 4.82 (tdd, *J* = 6.4, 6.1, 1.1 Hz, 1H), 3.85 (d, *J* = 1.0 Hz, 6H), 3.82 (d, *J* = 0.9 Hz, 3H), 1.47 (dd, *J* = 6.5, 0.9 Hz, 3H).

Figure S14. ^{1}H NMR spectrum of Table 1 Entry 8 product **12a** in CDCl$_3$. Data are consistent with a commercial compound.

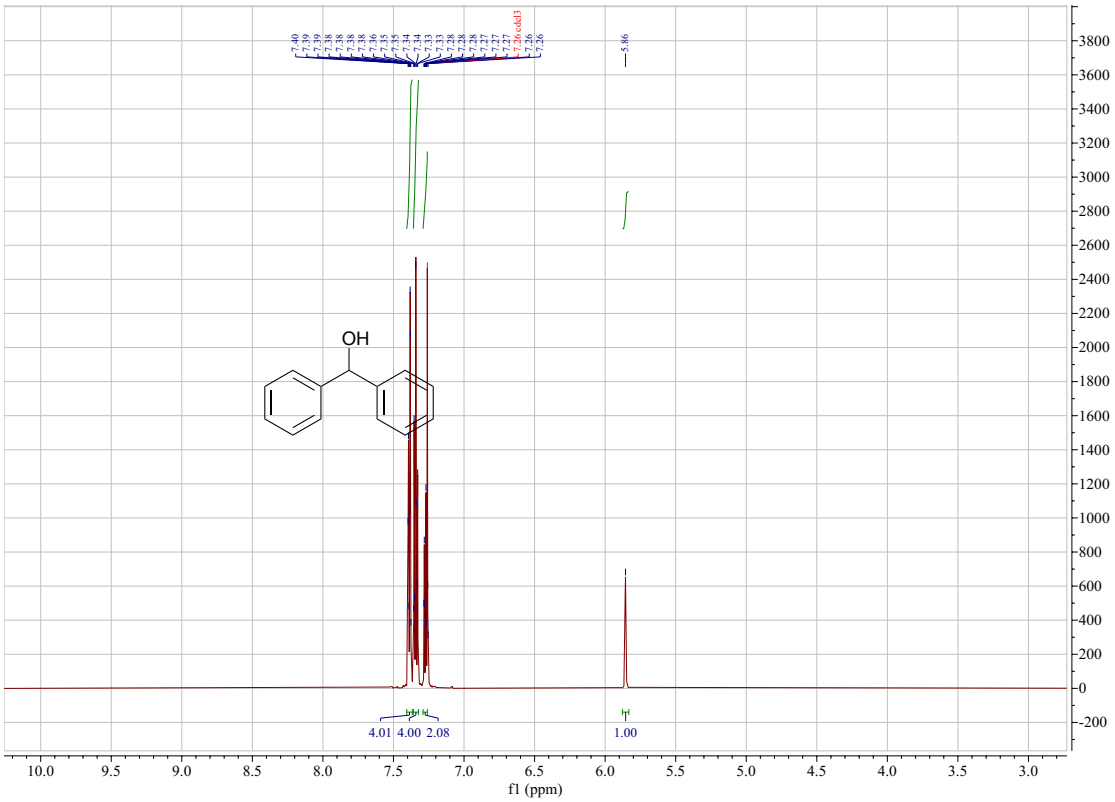

^{1}H NMR (600 MHz, cdcl$_3$) δ 7.41 – 7.36 (m, 4H), 7.34 (dd, J = 8.5, 6.8 Hz, 4H), 7.30 – 7.26 (m, 2H), 5.86 (s, 1H).

Figure S15. ^{1}H NMR spectrum of Table 1 Entry 9 product **13a** in CDCl$_3$. Data are consistent with a commercial compound.

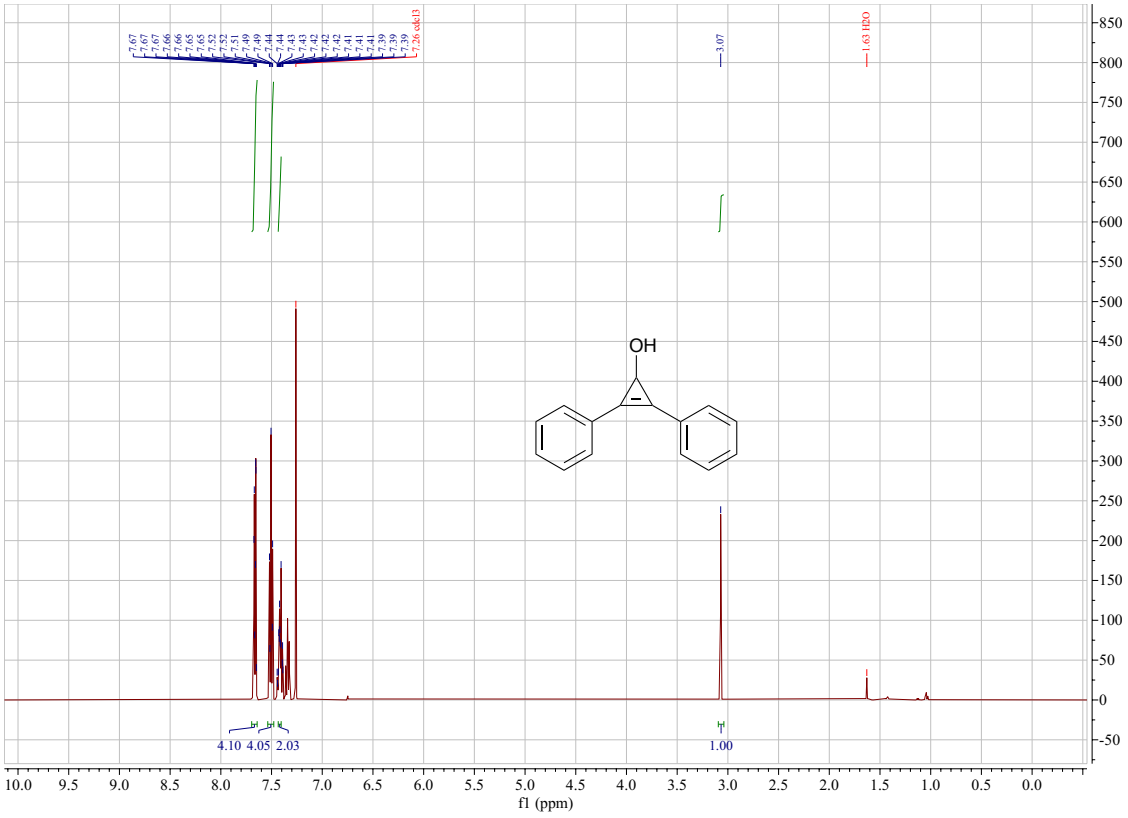

^{1}H NMR (500 MHz, cdcl$_3$) δ 7.69 – 7.64 (m, 4H), 7.50 (t, J = 7.7 Hz, 4H), 7.43 – 7.40 (m, 2H), 3.07 (s, 1H).

Figure S16. ^{1}H NMR spectrum of Table 1 Entry 10 product **14a** in CDCl$_3$. Data are consistent with a known compound.[3]

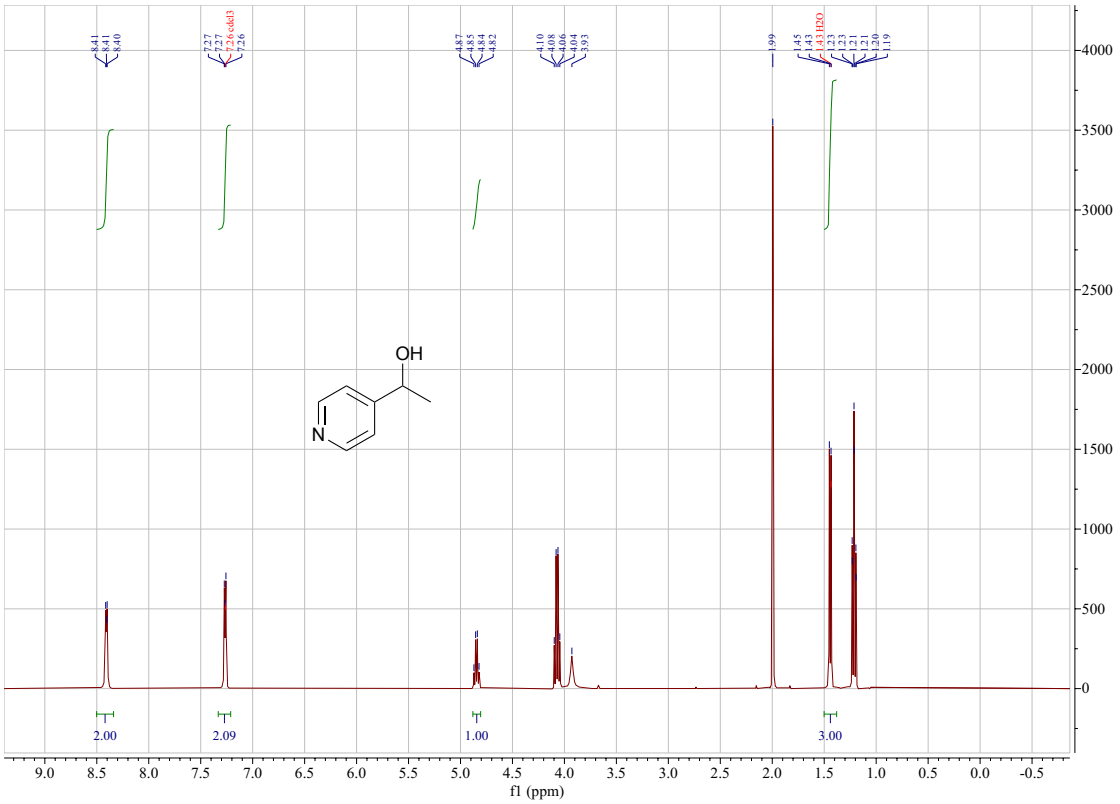

^{1}H NMR (400 MHz, cdcl$_3$) δ 8.51 – 8.31 (m, 2H), 7.34 – 7.19 (m, 2H), 4.85 (q, *J* = 6.5 Hz, 1H), 1.45 (d, *J* = 6.5 Hz, 3H).

Figure S17. ^{1}H NMR spectrum of Table 1 Entry 11 product **15a** in CDCl$_3$. Data are consistent with a commercial compound.

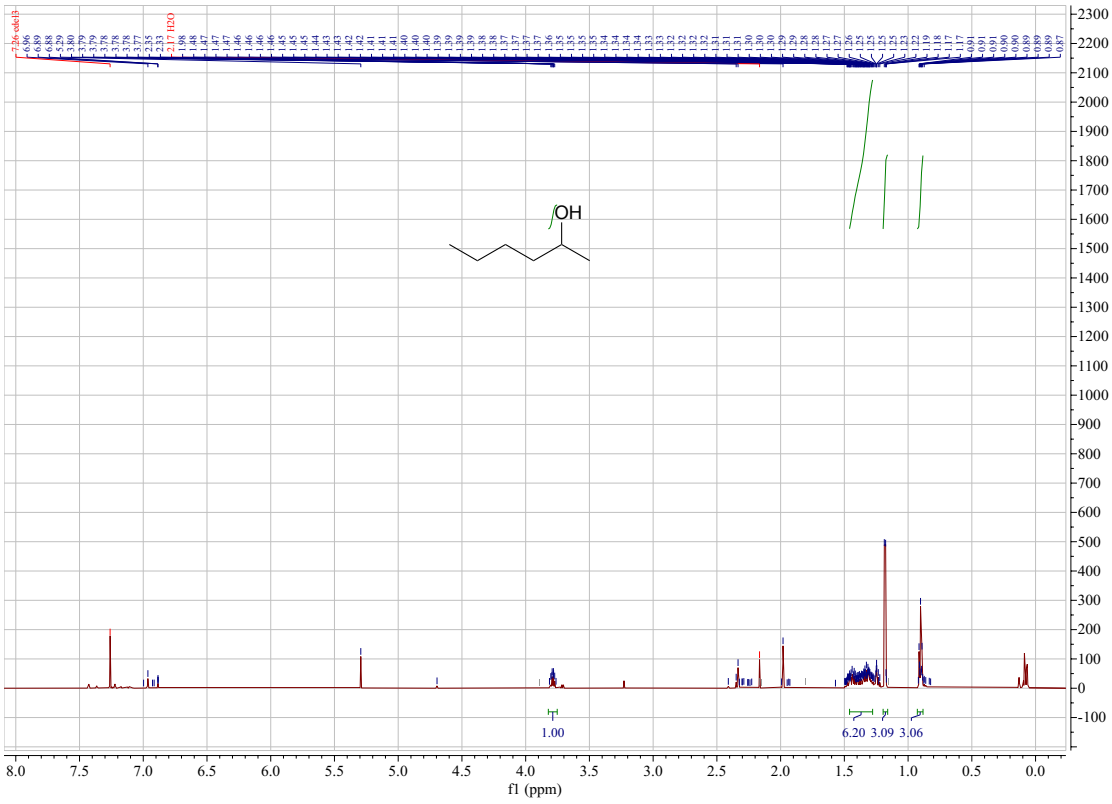

^{1}H NMR (600 MHz, cdcl$_3$) δ 3.83 – 3.74 (m, 1H), 1.47 – 1.28 (m, 6H), 1.18 (d, *J* = 6.2 Hz, 3H), 0.92 – 0.89 (m, 3H).

Figure S18. ^{1}H NMR spectrum of Table 1 Entry 12 product **16a** in CDCl$_3$. Data are consistent with a commercial compound.

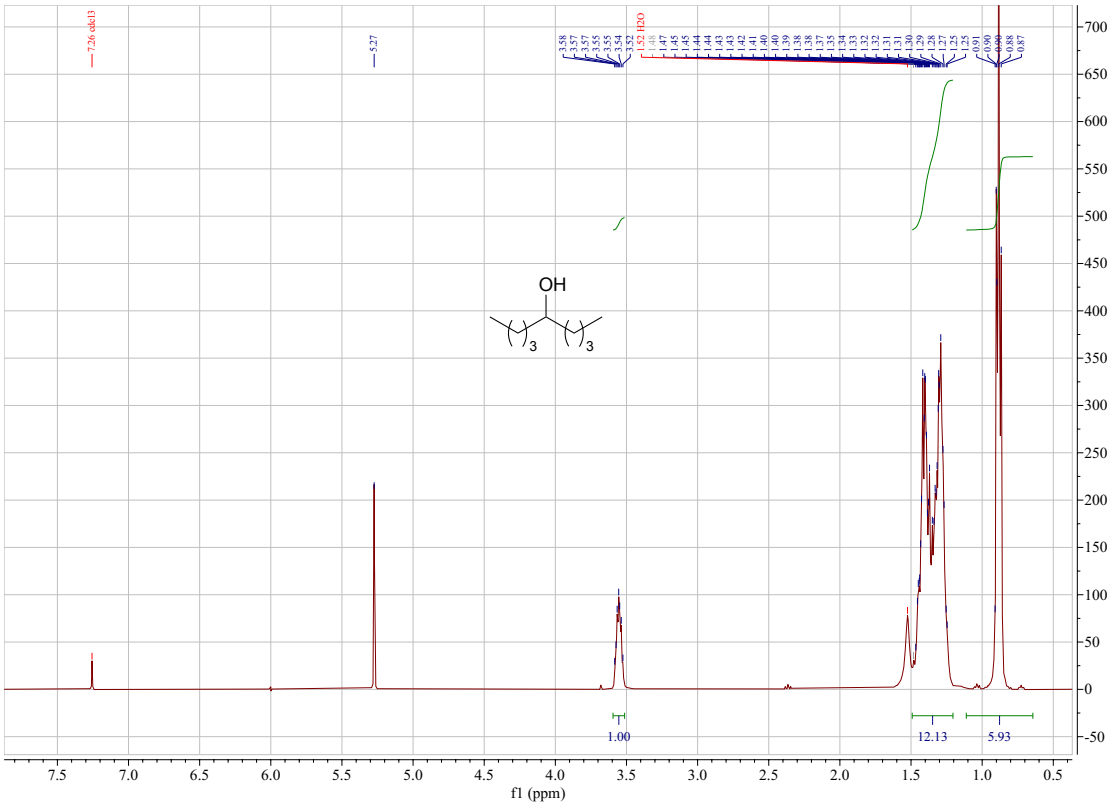

^{1}H NMR (400 MHz, cdcl$_3$) δ 3.56 (h, *J* = 4.3 Hz, 1H), 1.49 – 1.21 (m, 12H), 0.98 – 0.80 (t, 6H).

Figure S19. ^{1}H NMR spectrum of Table 1 Entry 13 product **17a** in $CDCl_3$. Data are consistent with a commercial compound.

Entry 14 product **18a**:

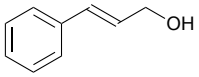

^{1}H NMR (400 MHz, cdcl$_3$) δ 7.37 (d, *J* = 7.2 Hz, 2H), 7.34 – 7.27 (m, 3H), 6.59 (dd, *J* = 15.8, 1.7 Hz, 1H), 6.35 (dt, *J* = 15.9, 5.7 Hz, 1H), 4.30 (dd, *J* = 5.7, 1.6 Hz, 2H).

Entry 15 product **19a**:

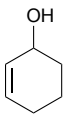

^{1}H NMR (400 MHz, cdcl$_3$) δ 5.90 – 5.87 (t, 1H), 5.76 – 5.73 (t, 1H), 4.06 (t, 1H), 2.08 – 2.04 (m, 2H), 1.87 – 1.83 (m, 2H), 1.73 – 1.69 (m, 2H).

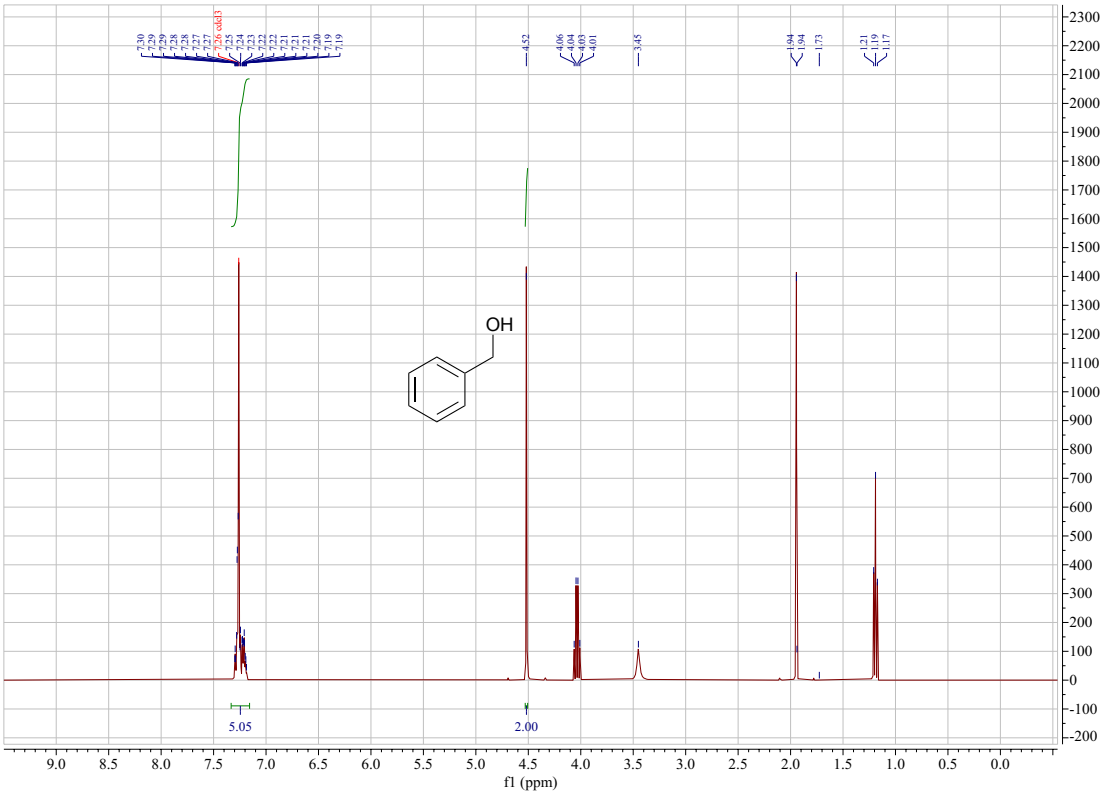

^{1}H NMR (400 MHz, cdcl$_3$) δ 7.50 – 7.04 (m, 5H), 4.52 (s, 2H).

Figure S20. ^{1}H NMR spectrum of Table 1 Entry 16 product **20a** in $CDCl_3$. Data are consistent with a commercial compound.

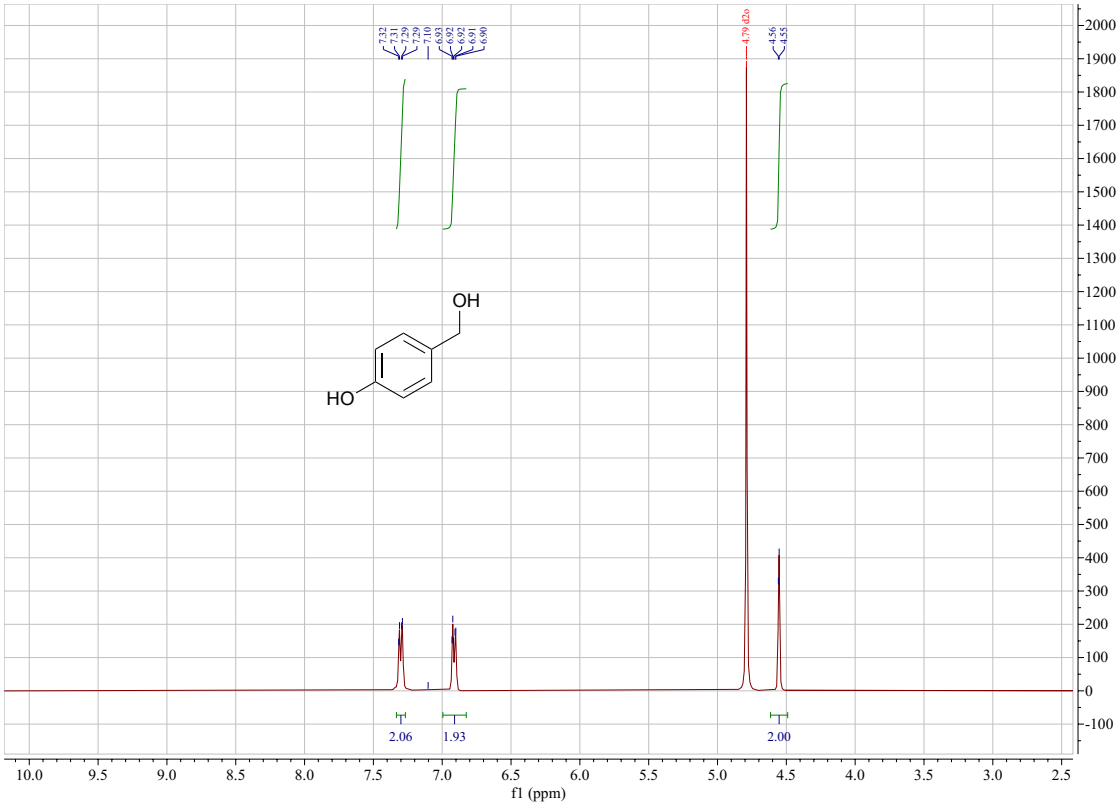

^{1}H NMR (400 MHz, d$_2$o) δ 7.30 (dd, *J* = 8.5, 2.3 Hz, 2H), 7.00 – 6.83 (m, 2H), 4.55 (d, *J* = 2.2 Hz, 2H).

Figure S21. ^{1}H NMR spectrum of Table 1 Entry 17 product **21a** in D_2O. Data are consistent with a commercial compound.

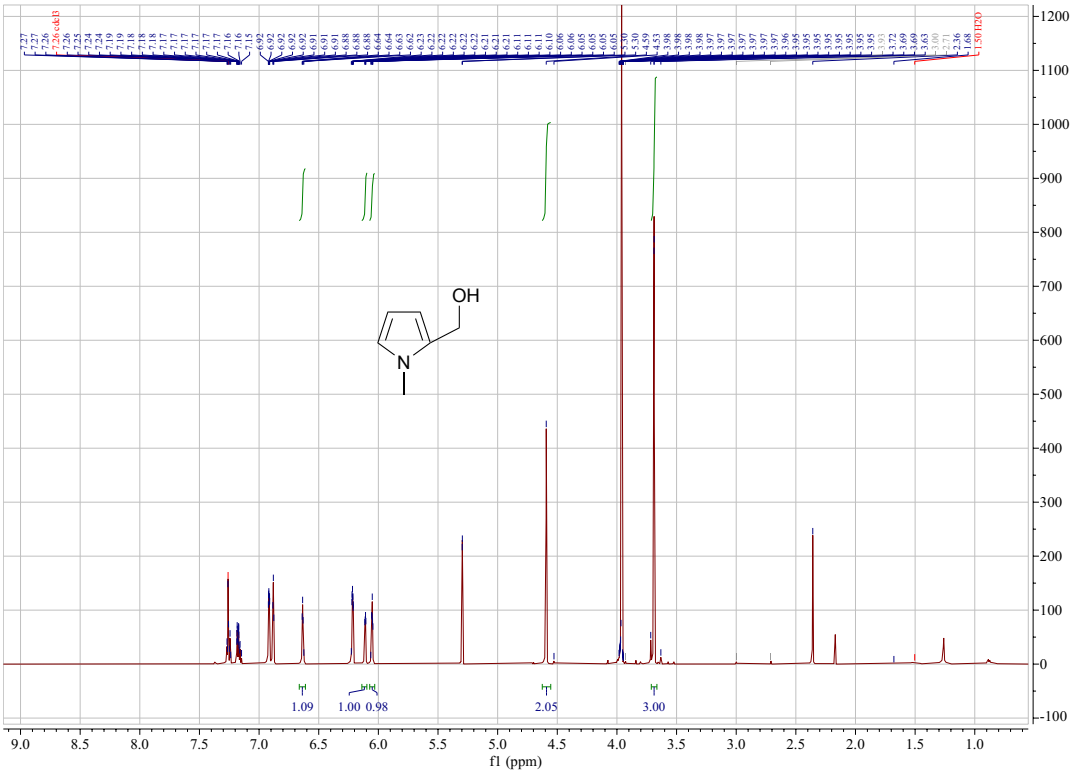

^{1}H NMR (600 MHz, cdcl$_3$) δ 6.67 – 6.61 (m, 1H), 6.11 (dd, *J* = 3.6, 1.8 Hz, 1H), 6.05 (dd, *J* = 3.5, 2.7 Hz, 1H), 4.59 (s, 2H), 3.69 (s, 3H).

Figure S22. ^{1}H NMR spectrum of Table 1 Entry 18 product **22a** in $CDCl_3$. Data are consistent with a commercial compound.

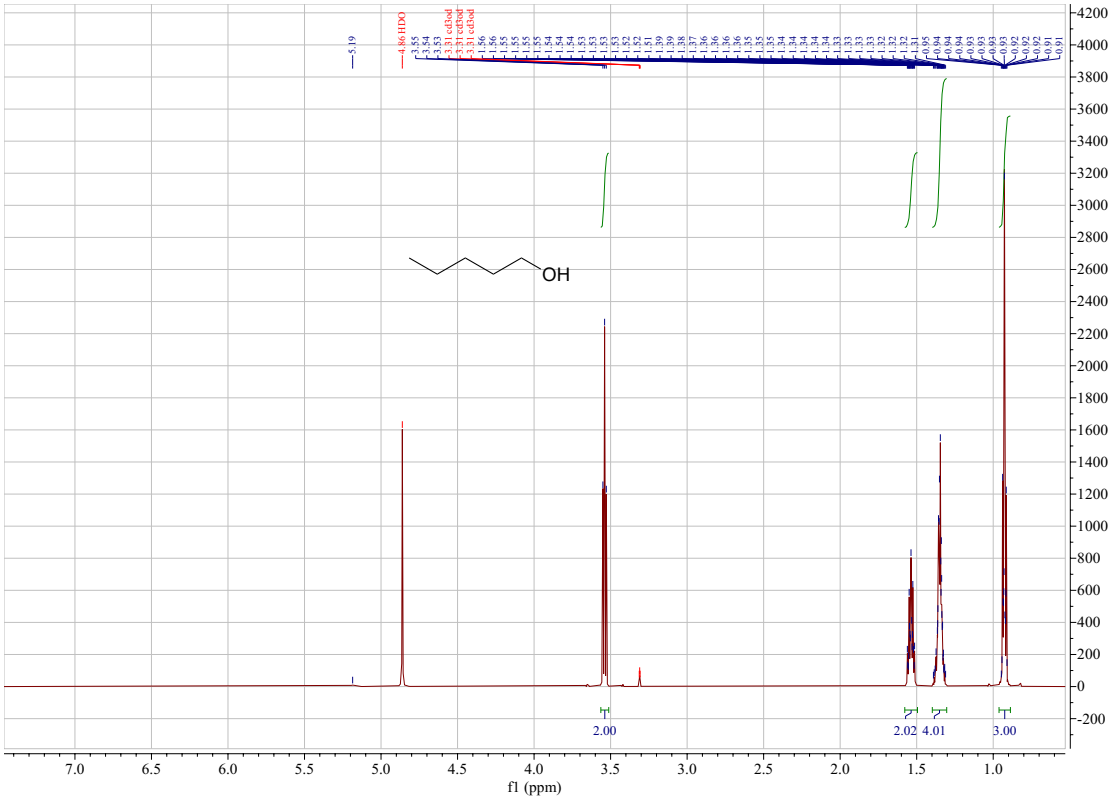

^{1}H NMR (600 MHz, cd$_3$od) δ 3.54 (t, *J* = 6.7 Hz, 2H), 1.58 – 1.49 (m, 2H), 1.40 – 1.30 (m, 4H), 0.96 – 0.89 (m, 3H).

Figure S23. ^{1}H NMR spectrum of Table 1 Entry 19 product **23a** in CD_3OD. Data are consistent with a commercial compound.

V. Mechanistic Study

Catalyst Initiation

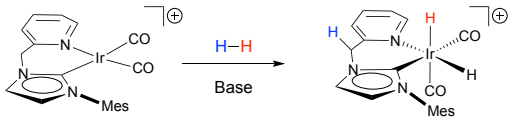

1 **5**

In a glovebox, iridium compound **1** (20 mg, 0.030 mmol) and KO^{t}Bu (11.0 mg, 3.3 eq) are added to a J. Young tube. dichloromethane-d_2 (1.0 mL) solvent is added to dissolve the solid mixture. J. Young tube is then gently evacuated, refilled with 1 atm H_2 and placed at room temperature for 10 min. ^{1}H NMR shows a kind of Ir-dihydride (compound **5**) formed (Figure S26). Data are consistent with a known compound.[4] CCDC# 2142636 contains supplementary crystallographic data for **5**.

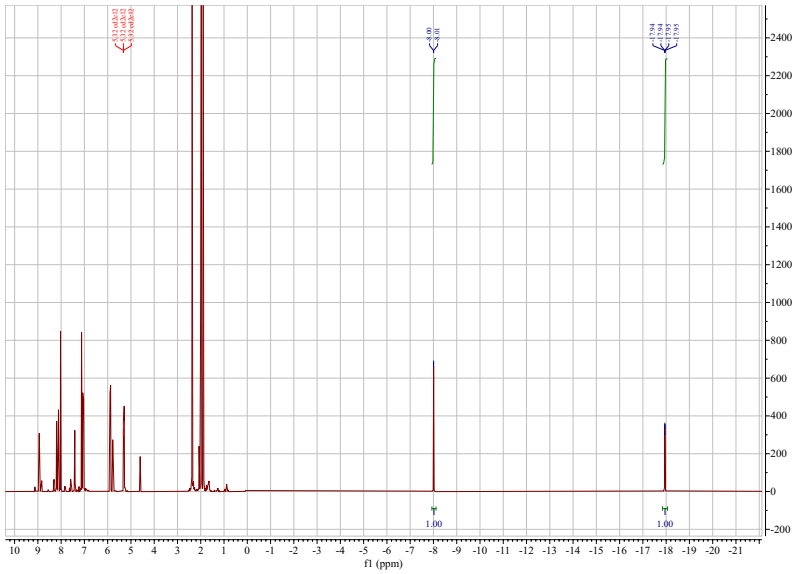

Figure S24. ^{1}H NMR spectrum of compound **5** in CD_2Cl_2.

In a glovebox, iridium compound **6** (20 mg, 0.038 mmol) and NaOH (4.6 mg, 3.3 eq) are added to a J. Young tube. Acetonitrile-d_3 (1.0 mL) solvent is added to dissolve the solid mixture. J. Young tube is then gently evacuated, refilled with 1 atm H_2 and placed at room temperature for 60 min. ^{1}H NMR shows three Ir-H signals (Figure S27).

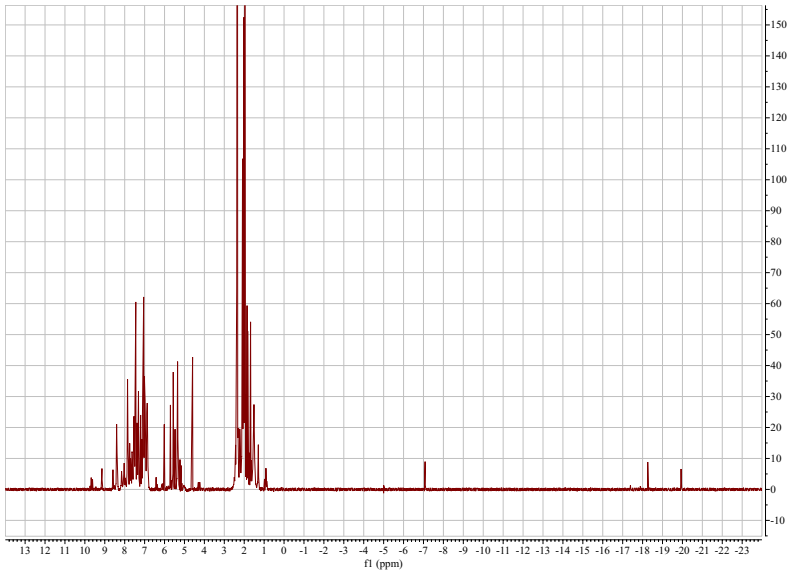

Figure S25. ^{1}H NMR spectrum of Ir-H species in CD_2Cl_2.

Reaction orders

Kinetic dependence on ketone concentration

In a glovebox, four different amounts of acetone (0.01mL, 0.138 mmol, or 0.02 mL, 0.276 mmol, or 0.03 mL, 0.414 mmol, or 0.04 mL, 0.552 mmol), iridium compound **1** (1.86 mg, 0.032 mmol) and KO^{t}Bu (1.03 mg, 0.009 mmol) are added to a J. Young tube. Toluene-d_8 (1.0 mL) is added to dissolve the solid mixture. The J. Young tube is then gently evacuated, refilled with 1 atm H_2. The NMR tube is heated to 100 °C for a kinetic run. Rate constant of each kinetic run is calculated based on the consumption of the acetone substrate. Rate constants are calculated to be 5.0(1) × 10^{-6} s^{-1}, 5.1(2) × 10^{-6} s^{-1}, 4.2(9) × 10^{-6} s^{-1}, 4.8(5) × 10^{-6} s^{-1} (figure S28). A log-log plot (figure S29) gives us a slop of 0.94(5), indicating the reaction is first order on the ketone substrate.

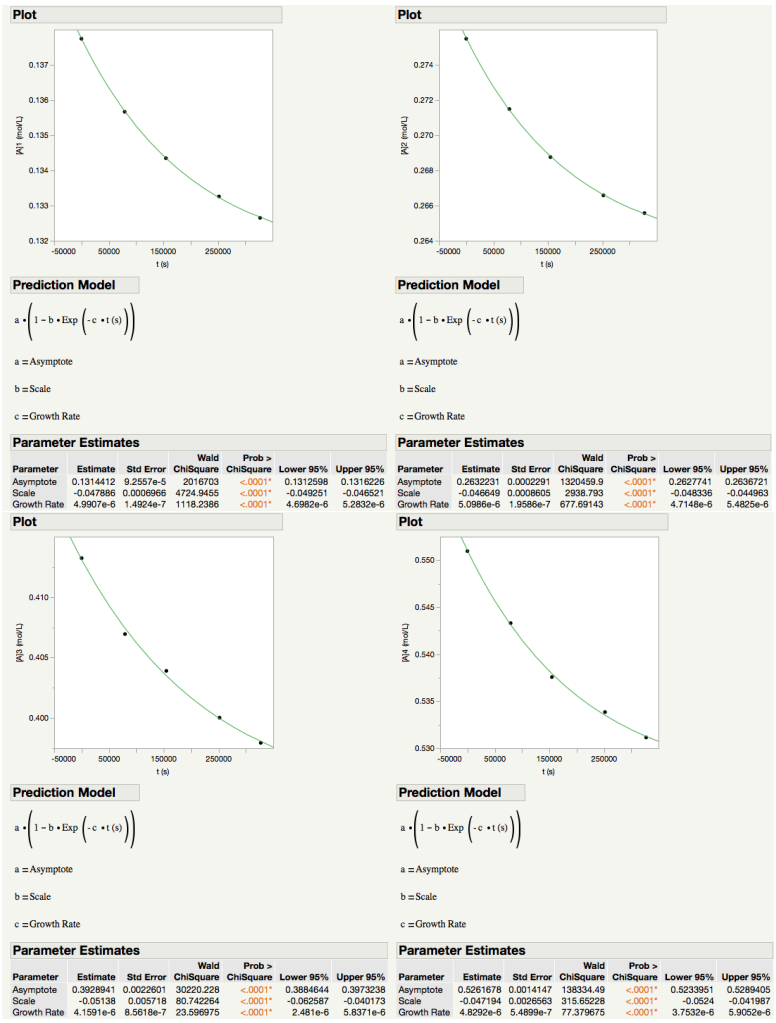

Figure S26. Kinetic profile of hydrogenation of four different amounts of acetone.

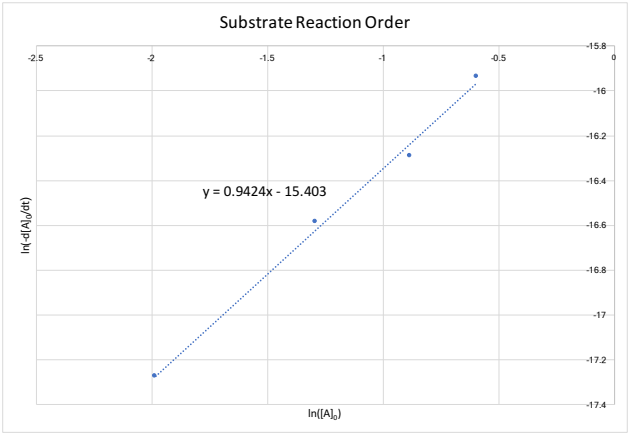

Figure S27. Kinetic dependence of acetone.

Kinetic dependence on base concentration

In a glovebox, four different amounts of KO^{t}Bu (1.5 mg, 0.0138 mmol, or 3.0 mg, 0.0276 mmol, or 4.5 mg, 0.0414 mmol, or 6.0 mg, 0.0552 mmol), iridium compound **1** (5.6 mg, 0.008 mmol) and acetone (0.02 mL, 0.276 mmol) are added to a J. Young tube. Toluene-d_8 (1.0 mL) is added to dissolve the solid mixture. The J. Young tube is then gently evacuated, refilled with 1 atm H_2. The NMR tube is heated to 100 °C for a kinetic run. Rate constant of each kinetic run is calculated based on the consumption of the acetone substrate. Rate constants are calculated to be 5.0(1) × 10^{-6} s^{-1}, 5.3(3) × 10^{-6} s^{-1}, 5.0(1) × 10^{-6} s^{-1}, 5.0(1) × 10^{-6} s^{-1} (figure S30). A log-log plot (figure S31) gives us a slop of 0.76(12), indicating the reaction is first order on the base KO^{t}Bu.

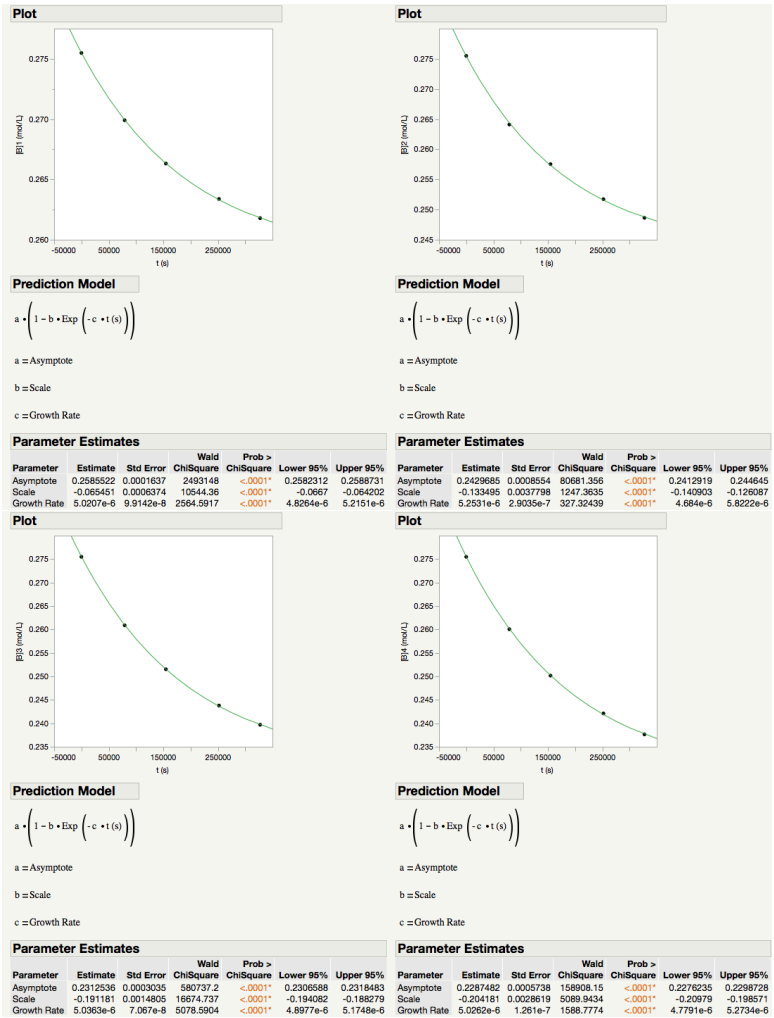

Figure S28. Kinetic profile of hydrogenation of acetone using four different amounts of base.

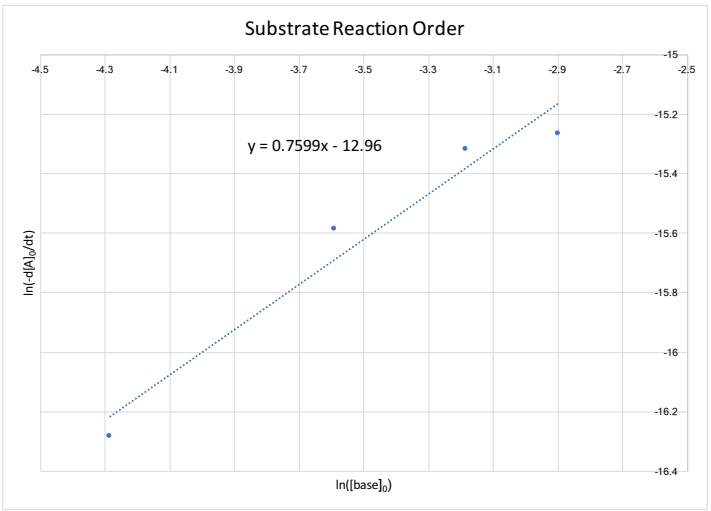

Figure S29. Kinetic dependence of base.

Kinetic dependence on catalyst concentration

In a glovebox, four different amounts of iridium compound **1** (0.93 mg, 0.00138 mmol, or 4.65 mg, 0.0069 mmol, or 9.3 mg, 0.0138 mmol, or 18.6 mg, 0.0276 mmol), KO^{t}Bu (10.1 mg, 0.09 mmol) and acetone (0.02 mL, 0.276 mmol) are added to a J. Young tube. Toluene-d_8 (1.0 mL) is added to dissolve the solid mixture. The J. Young tube is then gently evacuated, refilled with 1 atm H_2. The NMR tube is heated to 100 °C for a kinetic run. Rate constant of each kinetic run is calculated based on the consumption of the acetone substrate. Rate constants are calculated to be 5.1(2) × 10^{-6} s^{-1}, 5.2(3) × 10^{-6} s^{-1}, 5.0(2) × 10^{-6} s^{-1}, 5.3(3) × 10^{-6} s^{-1} (figure S32). A log-log plot (figure S33) gives us a slop of 0.88(4), indicating the reaction is first order on the iridium compound **1**.

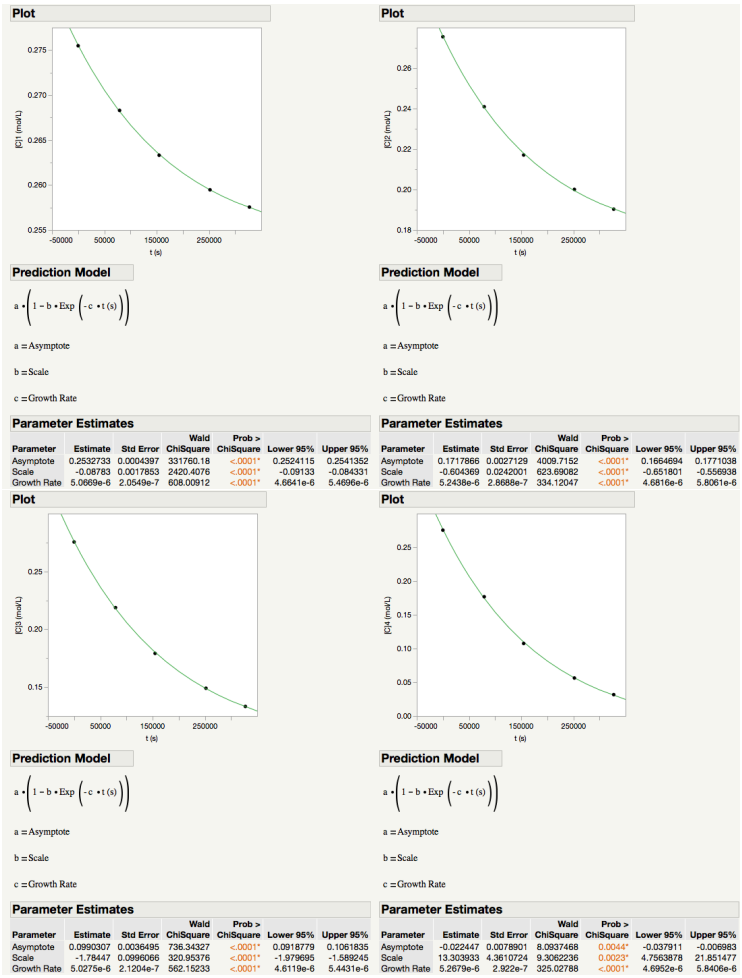

Figure S30. Kinetic profile of hydrogenation of acetone using four different amounts of catalyst **1**.

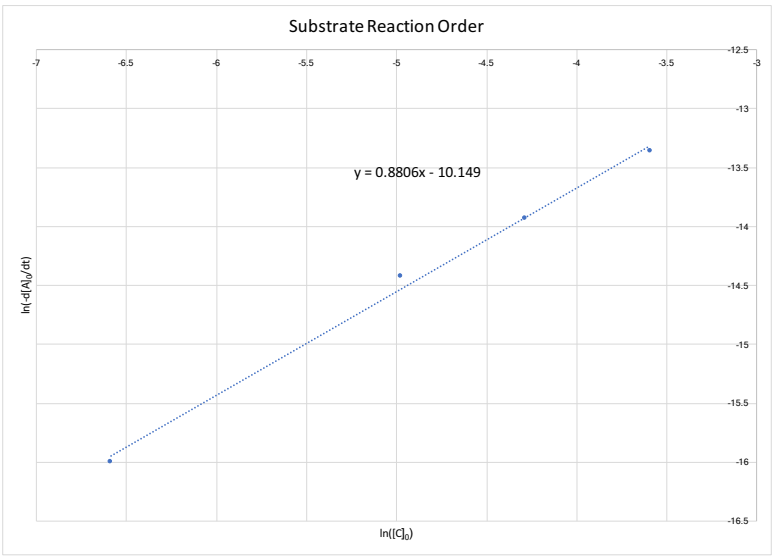

Figure S31. Kinetic dependence of catalyst **1**.

KIE Study

In a glovebox, benzophenone (16 mg, 0.0878 mmol), iridium catalyst **1** (1.78 mg, 0.00263 mmol, 3 mol %) and KO^{t}Bu (0.99 mg, 0.00878 mmol) are added to a J. Young tube. Toluene-d_8 (1.0 mL) is added to dissolve the solid mixture. The J. Young tube is then gently evacuated, refilled with 1 atm H_2 or D_2 and heated to 100 °C for a kinetic study. Rate constant of each kinetic run is calculated based on the consumption of the benzophenone substrate (figure S33). For the H_2 experiment, a rate constant of 5.3(3) × 10^{-6} s^{-1} could be obtained, while for the D_2 run, we observed a rate constant of 5.6(4) × 10^{-6} s^{-1}. This gives us a $KIE_{H2/D2}$ = 1.06(11).

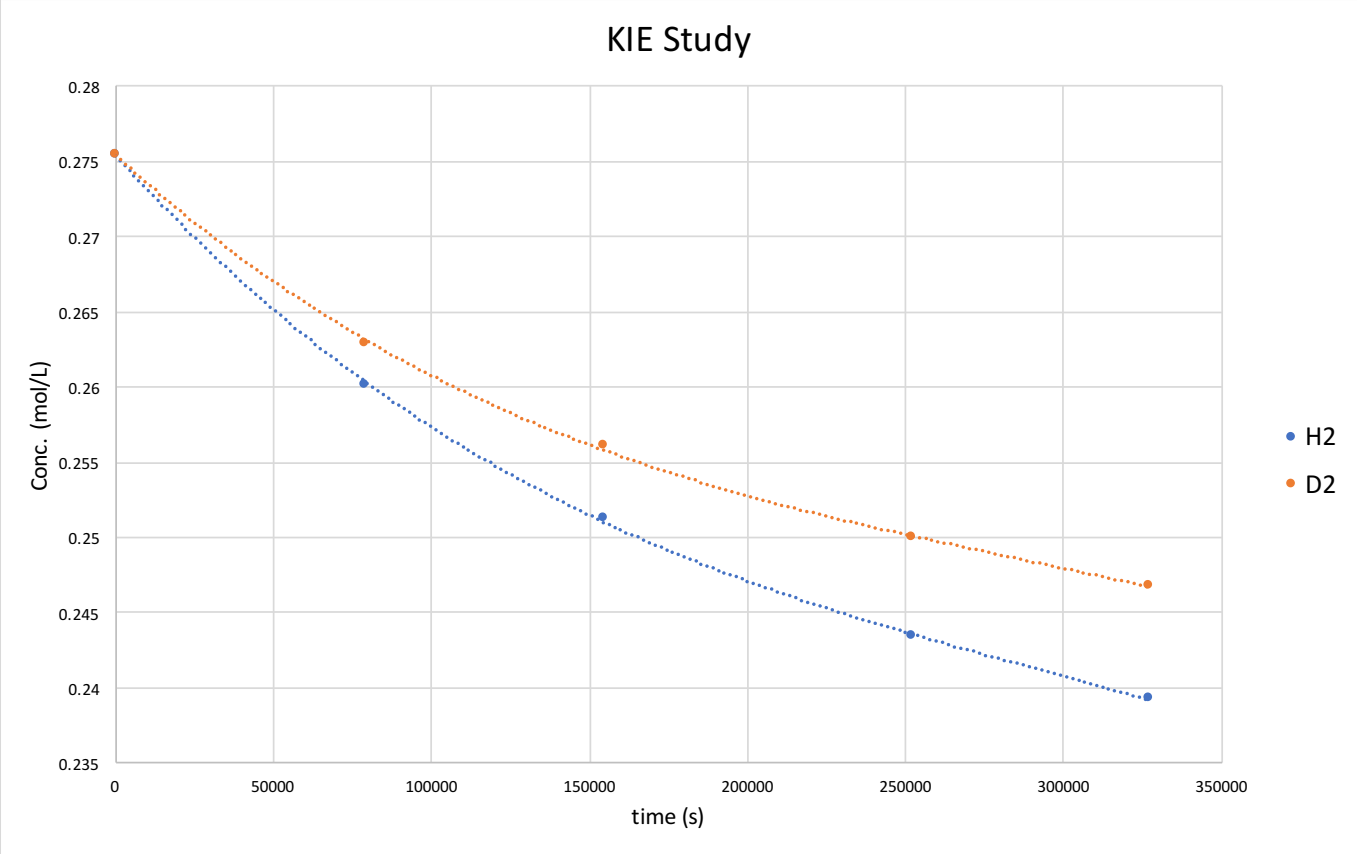

Figure S32. KIE study of benzophenone hydrogenation by catalyst **1**.

Hammett Analysis

In four parallel runs, 0.06 mmol substrates (acetophenone or 4'-methoxyacetophenone or 4'-chloroacetophenone or 4'-bromoacetophenone or 4'-nitroacetophenone), iridium catalyst **1** (1.2 mg, 1.8×10^{-3} mmol) and KO^{t}Bu (0.67 mg, 6.0×10^{-3} mmol) are added to a J. Young tube. 1.0 mL toluene-d_8 is added to dissolve the solid mixture. The J. Young tube is then gently evacuated, refilled with 1 atm H_2. The NMR tube is heated to 100 °C for a kinetic run (Figure S35). The Hammett plot (Figure S36) gives us the reaction constant $\rho = -0.93$.

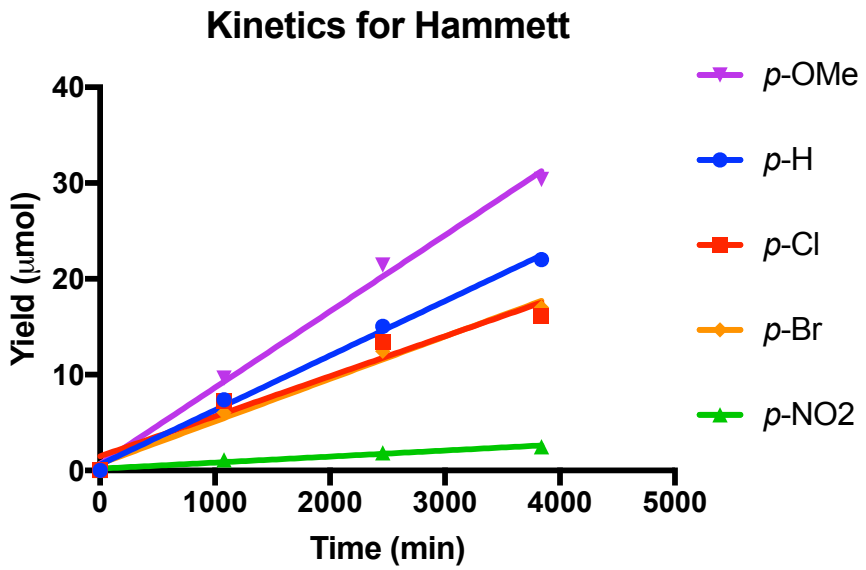

Figure S33. Kinetic profile of hydrogenation of a series of para-substituted acetophenones with different hydride affinities.

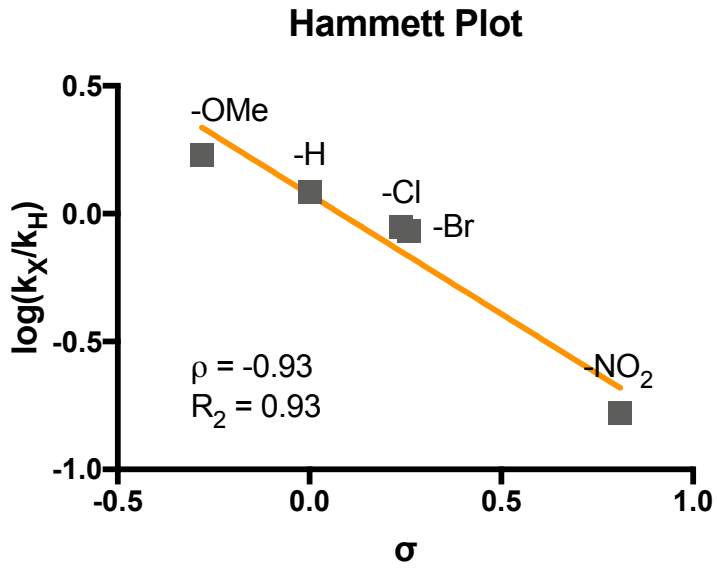

Figure S34. Hammett plot of hydrogenation of a series of para-substituted acetophenones with different hydride affinities.

Eyring Plot

In a glovebox, benzophenone (16 mg, 0.0878 mmol), iridium catalyst **1** (1.78 mg, 2.6 × 10^{-3} mmol, 3 mol %) and KO^{t}Bu (0.3 mg, 2.63× 10^{-3} mmol) are added to a J. Young tube. 1.0 mL toluene-d_8 is added to dissolve the solid mixture. The J. Young tube is then gently evacuated, refilled with 1 atm H_2. The tubes are heated to four temperatures (60 °C or 70 °C or 75 °C or 90°C) for kinetic runs. Rate constant of each kinetic run is calculated based on the consumption of the acetone substrate. A plot (figure S37) gives us the ΔH^{++} = +9.5(7) kcal mol^{-1} and ΔS^{++} = -42.8(25) cal mol^{-1} K^{-1}.

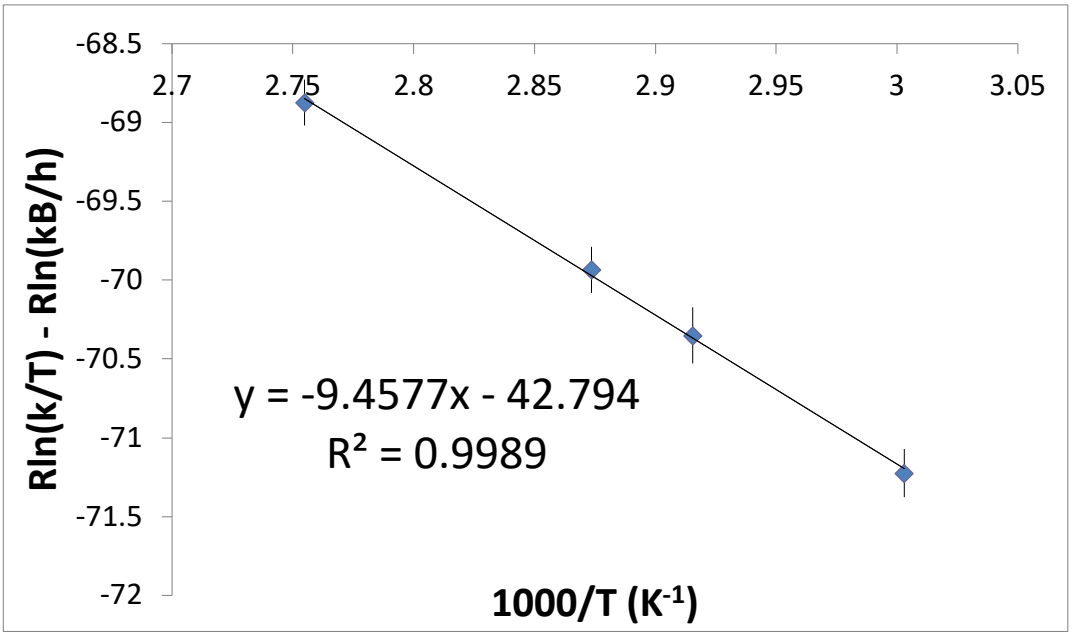

Figure S35. Eyring plot of benzophenone hydrogenation by catalyst **1**.

Proton Shuttle

In a glovebox, iridium compound **1** (2.6 mg, 0.00386 mmol), KO^{t}Bu (1.4 mg, 0.013 mmol), 4'-dimethylaminoacetophenone (21 mg, 0.129 mmol) and isopropanol (0.01 mL, 0.131 mmol, 1 eq to ketone substrate or 0 mL) are added to a J. Young tube. Toluene-d_8 (1.0 mL) is added to dissolve the solid mixture. The J. Young tube is then gently evacuated, refilled with 1 atm H_2. The NMR tube is heated to 100 °C for a kinetic run. Rate constant of each kinetic run is calculated based on the consumption of the ketone substrate. Rate constants are calculated to be 3.9(1) × 10^{-6} s^{-1} and 2.4(6) × 10^{-6} s^{-1} (figure S38). This gives us a ratio of these two different reaction rates $k_{ROH}/k_{no\ ROH}$ = 1.625.

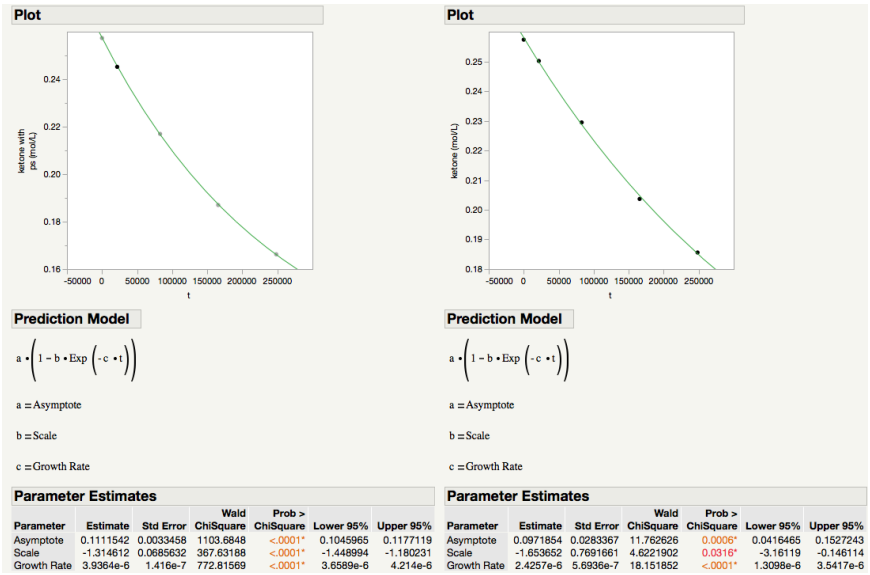

Figure S36. Kinetic profile of hydrogenation of 4'-dimethylaminoacetophenone with or without alcohol.

VI. Crystal Structure of **6**

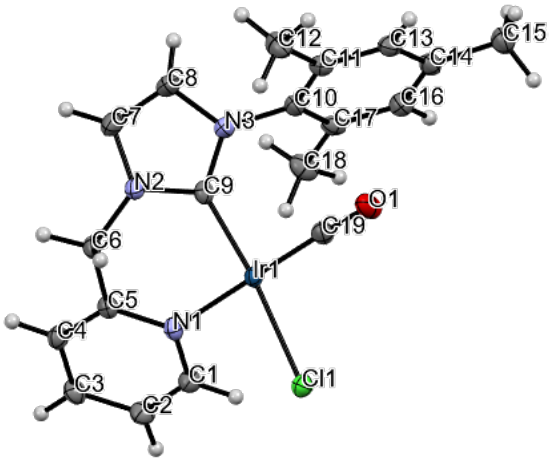

Figure S37. Molecular structure of **6**.

Yellow single crystals of $C_{19}H_{19}ClIrN_3O$ **[6]** were prepared from slow liquid diffusion of dichloromethane and diethyl ether. A suitable crystal was selected and mounted on a loop on a XtaLAB Mini II diffractometer. The crystal was kept at 100.00(10) K during data collection. The X-ray intensity data were measured on a Bruker APEX DUO system equipped with a fine-focus tube (MoK α , λ = 0.71073 Å) and a TRIUMPH curved-crystal monochromator.

Table S2. Crystal data and structure refinement for **6**.

Identification code	Iridium CN carbonyl chloride
Empirical formula	$C_{19}H_{19}ClIrN_3O$
Formula weight	533.02
Temperature/K	100.00(10)
Crystal system	monoclinic
Space group	$P2_1/c$
a/Å	8.7180(2)
b/Å	15.1641(3)
c/Å	14.4976(3)
α/°	90
β/°	106.108(2)
γ/°	90
Volume/Å^3	1841.35(7)
Z	4
ρ_{calc}g/cm^3	1.923

μ/mm^{-1}	7.408
F (000)	1024.0
Crystal size/mm^3	0.173 × 0.095 × 0.058
Radiation	Mo Kα (λ = 0.71073)
2Θ range for data collection/°	5.372 to 64.818
Index ranges	-13 ≤ h ≤ 12, -22 ≤ k ≤ 20, -20 ≤ l ≤ 21
Reflections collected	50998
Independent reflections	5943 [R_{int} = 0.0498, R_{sigma} = 0.0296]
Data/restraints/parameters	5943/0/232
Goodness-of-fit on F^2	1.041
Final R indexes [I>=2σ (I)]	R_1 = 0.0251, wR_2 = 0.0457
Final R indexes [all data]	R_1 = 0.0377, wR_2 = 0.0501
Largest diff. peak/hole / e Å^{-3}	2.65/-1.10

Table S3. Fractional Atomic Coordinates (×10^4) and Equivalent Isotropic Displacement Parameters (Å^2×10^3) for Iridium CN Carbonyl Chloride. U_{eq} is defined as 1/3 of the trace of the orthogonalised U_{IJ} tensor.

Atom	*x*	*y*	*z*	U(eq)
Ir1	3407.11(13)	7004.50(7)	6358.82(8)	15.41(4)
Cl1	1781.1(9)	8218.5(5)	5624.7(6)	22.14(15)
O1	903(3)	6376.5(17)	7228(2)	33.7(6)
N1	4774(3)	5210.1(18)	7182(2)	20.4(5)
N2	6544(3)	6203.4(18)	7216.6(19)	18.6(5)
N3	5147(3)	7429.4(17)	5672.3(19)	17.7(5)
C1	4665(4)	7684(2)	4748(2)	20.7(6)
C2	5719(4)	7884(2)	4221(2)	23.3(7)
C3	7343(4)	7843(2)	4663(2)	23.5(7)
C4	7854(4)	7578(2)	5615(2)	20.1(6)
C5	6738(4)	7374(2)	6100(2)	17.1(6)
C6	7234(3)	7063(2)	7125(2)	18.7(6)
C7	7366(4)	5452(2)	7609(3)	26.5(7)
C8	6262(4)	4831(2)	7591(3)	26.6(7)
C9	4938(4)	6074(2)	6948(2)	18.0(6)
C10	3274(4)	4756(2)	7031(2)	20.4(6)
C11	2702(4)	4596(2)	7827(2)	21.1(6)
C12	3605(5)	4880(3)	8827(2)	30.5(8)
C13	1226(4)	4174(2)	7666(2)	21.3(6)
C14	360(4)	3906(2)	6757(2)	21.4(6)
C15	-1192(4)	3421(2)	6599(3)	28.4(7)
C16	978(4)	4081(2)	5981(2)	21.8(6)
C17	2434(4)	4500(2)	6102(2)	20.2(6)
C18	3091(5)	4666(2)	5262(3)	27.7(7)
C19	1899(4)	6611(2)	6896(3)	22.1(6)

Table S4. Anisotropic Displacement Parameters (Å^2×10^3) for Iridium CN Carbonyl Chloride. The Anisotropic displacement factor exponent takes the form: $-2\pi^2[h^2a^{*2}U_{11}+2hka^*b^*U_{12}+\ldots]$.

Atom	U_{11}	U_{22}	U_{33}	U_{12}	U_{13}	U_{23}
Ir1	12.66(5)	16.78(6)	17.60(6)	-0.37(4)	5.54(4)	-0.14(5)
Cl1	17.6(3)	21.9(4)	27.9(4)	2.9(3)	8.0(3)	3.3(3)
O1	26.5(13)	28.8(13)	55.3(18)	6.4(10)	27.0(13)	12.9(12)
N1	17.1(12)	19.3(13)	24.7(14)	1.8(10)	5.8(10)	4.7(11)
N2	14.7(12)	21.9(13)	19.7(13)	0.4(10)	5.6(10)	2.6(10)
N3	15.4(12)	18.7(12)	20.4(13)	-1.1(9)	7.2(10)	-2.6(10)
C1	20.1(15)	23.2(15)	19.0(15)	1.3(12)	6.0(12)	0.5(12)
C2	25.3(16)	27.7(17)	19.2(15)	0.4(13)	9.9(13)	3.0(13)
C3	22.2(15)	27.3(17)	25.0(16)	-1.0(12)	13.5(13)	2.4(13)
C4	16.0(14)	22.0(15)	24.1(16)	0.7(11)	8.4(12)	-0.2(12)

Table S4. Anisotropic Displacement Parameters ($Å^2×10^3$) for Iridium CN Carbonyl Chloride. The Anisotropic displacement factor exponent takes the form: $-2\pi^2[h^2a^{*2}U_{11}+2hka^*b^*U_{12}+\ldots]$.

Atom	U_{11}	U_{22}	U_{33}	U_{12}	U_{13}	U_{23}
C5	16.7(14)	17.8(14)	17.5(14)	-1.4(11)	5.7(11)	-2.8(11)
C6	13.5(13)	23.3(15)	19.1(14)	-3.3(11)	4.0(11)	0.5(12)
C7	18.3(15)	31.9(18)	29.0(18)	5.2(13)	6.2(13)	7.8(14)
C8	21.5(16)	23.9(17)	33.6(19)	5.9(13)	6.3(14)	8.8(14)
C9	16.6(13)	21.5(15)	16.4(14)	-0.9(11)	5.6(11)	-1.6(12)
C10	17.0(14)	17.3(14)	26.9(16)	-0.9(11)	6.2(12)	1.9(12)
C11	22.5(15)	19.1(15)	21.6(15)	0.2(12)	6.0(12)	3.7(12)
C12	34.5(19)	34.6(19)	20.1(16)	-9.6(16)	3.9(14)	0.9(14)
C13	22.8(15)	19.7(15)	22.8(16)	1.4(12)	8.8(13)	3.7(12)
C14	20.1(14)	17.5(14)	27.6(16)	-1.2(11)	8.3(13)	0.0(12)
C15	23.7(17)	26.2(17)	35(2)	-3.3(13)	7.9(14)	-0.5(15)
C16	23.1(15)	21.2(15)	20.8(15)	1.4(12)	5.8(12)	-2.0(12)
C17	24.1(15)	16.1(14)	23.2(16)	3.4(11)	11.1(13)	2.2(12)
C18	34.6(19)	26.0(17)	27.6(18)	-2.5(14)	17.5(15)	-2.1(14)
C19	20.9(15)	18.0(15)	27.9(17)	0.8(12)	7.8(13)	-1.1(13)

Table S5. Bond Lengths for Iridium CN Carbonyl Chloride.

Atom	Atom	Length/Å	Atom	Atom	Length/Å
Ir1	Cl1	2.3863(8)	C2	C3	1.384(5)
Ir1	N3	2.132(3)	C3	C4	1.387(5)
Ir1	C9	1.967(3)	C4	C5	1.384(4)
Ir1	C19	1.806(3)	C5	C6	1.504(4)
O1	C19	1.159(4)	C7	C8	1.342(5)
N1	C8	1.392(4)	C10	C11	1.399(5)
N1	C9	1.370(4)	C10	C17	1.398(5)
N1	C10	1.440(4)	C11	C12	1.508(5)
N2	C6	1.457(4)	C11	C13	1.398(5)
N2	C7	1.382(4)	C13	C14	1.386(5)
N2	C9	1.360(4)	C14	C15	1.501(5)
N3	C1	1.345(4)	C14	C16	1.400(5)
N3	C5	1.355(4)	C16	C17	1.387(5)
C1	C2	1.382(4)	C17	C18	1.503(5)

Table S6. Bond Angles for Iridium CN Carbonyl Chloride.

Atom	Atom	Atom	Angle/°	Atom	Atom	Atom	Angle/°
N3	Ir1	Cl1	88.30(7)	C5	C6	N2	111.0(2)
C9	Ir1	Cl1	174.06(9)	C8	C7	N2	106.5(3)
C9	Ir1	N3	86.24(11)	C7	C8	N1	107.3(3)
C19	Ir1	Cl1	91.94(11)	N1	C9	Ir1	133.5(2)
C19	Ir1	N3	177.44(13)	N2	C9	Ir1	122.8(2)
C19	Ir1	C9	93.62(14)	N2	C9	N1	103.7(3)
C9	N1	C8	110.6(3)	C11	C10	N1	118.3(3)
C10	N1	C8	124.5(3)	C17	C10	N1	119.3(3)
C10	N1	C9	124.9(3)	C17	C10	C11	122.4(3)
C7	N2	C6	126.5(3)	C12	C11	C10	122.2(3)
C9	N2	C6	121.4(3)	C13	C11	C10	117.6(3)
C9	N2	C7	112.0(3)	C13	C11	C12	120.2(3)
C1	N3	Ir1	119.1(2)	C14	C13	C11	121.8(3)
C5	N3	Ir1	122.6(2)	C15	C14	C13	121.2(3)
C5	N3	C1	118.1(3)	C16	C14	C13	118.6(3)
C2	C1	N3	122.8(3)	C16	C14	C15	120.2(3)

Table S6. Bond Angles for Iridium CN Carbonyl Chloride.

Atom	Atom	Atom	Angle/°	Atom	Atom	Atom	Angle/°
C3	C2	C1	119.0(3)	C17	C16	C14	121.9(3)
C4	C3	C2	118.6(3)	C16	C17	C10	117.7(3)
C5	C4	C3	119.5(3)	C18	C17	C10	121.3(3)
C4	C5	N3	121.9(3)	C18	C17	C16	121.0(3)
C6	C5	N3	116.6(3)	O1	C19	Ir1	178.1(3)
C6	C5	C4	121.5(3)				

Table S7. Torsion Angles for Iridium CN Carbonyl Chloride.

A	B	C	D	Angle/°	A	B	C	D	Angle/°
Ir1	N3	C1	C2	-173.3(2)	N2	C6	C5	N3	56.7(3)
Ir1	N3	C5	C4	174.1(2)	N2	C6	C5	C4	-122.3(3)
Ir1	N3	C5	C6	-4.9(2)	N3	C1	C2	C3	-1.7(4)
Ir1	C9	N1	C8	180.0(3)	N3	C5	C4	C3	-0.4(4)
Ir1	C9	N1	C10	-0.3(4)	C1	C2	C3	C4	1.8(4)
Ir1	C9	N2	C6	3.0(3)	C2	C3	C4	C5	-0.9(4)
Ir1	C9	N2	C7	-179.8(3)	C3	C4	C5	C6	178.5(3)
N1	C8	C7	N2	0.3(3)	C10	C11	C13	C14	1.1(4)
N1	C9	N2	C6	-177.4(2)	C10	C17	C16	C14	-0.7(4)
N1	C9	N2	C7	-0.2(3)	C11	C13	C14	C15	177.5(3)
N1	C10	C11	C12	-0.2(4)	C11	C13	C14	C16	-1.2(4)
N1	C10	C11	C13	178.5(3)	C13	C14	C16	C17	1.0(4)
N1	C10	C17	C16	-178.7(3)	C14	C16	C17	C18	178.7(3)
N1	C10	C17	C18	1.8(4)					

Table S8. Hydrogen Atom Coordinates ($Å \times 10^4$) and Isotropic Displacement Parameters ($Å^2 \times 10^3$) for Iridium CN Carbonyl Chloride.

Atom	*x*	*y*	*z*	U(eq)
H1	3552(4)	7728(2)	4444(2)	24.8(7)
H2	5334(4)	8046(2)	3564(2)	28.0(8)
H3	8092(4)	7994(2)	4322(2)	28.2(8)
H4	8963(4)	7537(2)	5932(2)	24.2(7)
H6a	6879(3)	7496(2)	7534(2)	22.5(7)
H6b	8413(3)	7024(2)	7351(2)	22.5(7)
H7	8491(4)	5388(2)	7846(3)	31.8(9)
H8	6458(4)	4242(2)	7816(3)	31.9(9)
H12a	4616(16)	4556(14)	9032(8)	45.7(12)
H12b	3820(30)	5514(4)	8830(5)	45.7(12)
H12c	2963(15)	4755(17)	9270(4)	45.7(12)
H13	805(4)	4067(2)	8194(2)	25.6(7)
H15a	-1098(11)	2835(7)	6335(19)	42.7(11)
H15b	-1451(17)	3359(16)	7212(4)	42.7(11)
H15c	-2042(8)	3752(9)	6148(16)	42.7(11)
H16	382(4)	3909(2)	5355(2)	26.1(7)
H18a	3270(30)	5299(3)	5209(12)	41.5(11)
H18b	4102(17)	4349(14)	5358(9)	41.5(11)
H18c	2325(15)	4458(16)	4672(4)	41.5(11)

VII. Reference

1. F. Cisnetti, P. Lemoine, M. El-Ghozzi, D. Avignant and A. Gautier, *Tetrahedron Letters*, 2010, **51**, 5226-5229.
2. O. Kaufhold, F.E. Hahn, T. Pape and A. Hepp, *Journal of Organometallic Chemistry*, 2008, **693**, 3435-3440.

3. K. Komatsu, M. Arai, Y. Hattori, K. Fukuyama, Y. Katsube and K. Okamoto, *The Journal of Organic Chemistry*, 1987, **52**, 2183-2192.
4. V. K. Do, N. Alfonso Vargas, A. J. Chavez, L. Zhang, V. Cherepakhin, Z. Lu, R. P. Currier, P. A. Dub, J. C. Gordon and T. J. Williams, *Catalysis Science & Technology*, 2022, **12**, 7182 – 7189.